HIGH TECH

SIMULATE ELECTRONIC DEVICE PERFORMANCE
WITH MULTIPHYSICS SIMULATION

Accelerating Electronic Device Development With Nonlinear Finite Element Analysis and Multiphysics Simulation

Content

Lenovo ThinkPads Get Tougher and More Sensitive with Abaqus FEA

SIMULIA's FEA software helps Lenovo design out flex, engineer in stiffness and improve keystroke feel

The LenovoThinkPad line of laptops is known for its striking aesthetics. The shape of the original IBM design was inspired by Japanese bento lunch boxes (a form still used in ThinkPads today). The 1995 ThinkPad 701, with its unique "butterfly" expanding keyboard, is in the collection of New York's Museum of Modern Art.

But most laptops don't sit safely in display cases, or even stay in one place. Consider a typical morning in a coffee shop: A college student strides to his table, bangs a laptop down, flips it open, and begins typing forcefully and enthusiastically. Nearby, another student slams her computer shut, picks it up with a one-handed squeeze, and dashes out at caffeine-induced speeds, bumping it against the doorframe.

> "With Abaqus, we're able to be more innovative, more quickly, and produce higher-quality products."
> —Dr. Zhifeng Xin, Lenovo

At Lenovo, a great deal of design effort goes into ensuring that "portable" doesn't mean "breakable." It's a measure of how seriously engineers take this task that two recent designs for the ThinkPad X300 and the T400 were code-named Kodachi and Shinai respectively—both the names of Japanese martial arts swords. Like those legendary weapons, ThinkPads are widely known for their performance and durability as well as looks—a legacy that Lenovo has continued since it purchased the laptop brand from IBM in 2005. "Our aim is to create a high-quality, reliably strong notebook while keeping cost and product development time down," says Dr. Zhifeng Xin, senior manager at the Lenovo Innovation Design Center (IDC) in Beijing.

The crucial phase of proving out new laptops is done by Lenovo's award-winning design center. In the past few years, the IDC has received a US Industrial Design Excellence Award (IDEA), Germany's Red Dot Best and iF Design Awards, Japan's international G-Mark Good Design Award for industrial design, and the Intel Innovation PC Award, among others.

Engineers at the IDC analyze all of Lenovo's products, ranging from PCs and notebooks to cell phones and servers. Finite element analysis (FEA) takes place at the concept, development, and failure analysis stages. FEA simulations at Lenovo include modeling drop, shock, vibration, static pressure, and motherboard strain.

The IDC also performs computational fluid dynamics thermal and airflow acoustic simulations.

Realistic simulation of notebook computers like the ThinkPad began at the IDC in 2007 and became a formal checkpoint in the product development process shortly thereafter. Abaqus has been an essential tool for FEA since the IDC first opened its simulation technology center. "With Abaqus, we're able to be more innovative, more quickly, and produce higher-quality products," Dr. Xin says.

Engineers use Abaqus early in design process to verify product strength, choose between different versions, and identify and improve problem areas. The process involves pre-processing from CAD to meshed model; establishing loads, boundaries, and part interactions; running the analysis; and creating the reports.

Flexible analysis, rigid results
FEA is especially central to eliminating flex, an objective vital to making the ThinkPad more reliable. A number of forces—such as carrying a closed notebook one-handed—can potentially deform the laptop frame and bend the motherboard, which could damage the soldered connections or the liquid crystal display (LCD). "Notebooks face

demanding loads and forces even when they're just being carried from place to place," says Dr. Xin. "It's important for the covers to be stiff enough, with minimal deformation, so that the rear cover will protect the display, while the base cover protects the motherboard."

During recent work on a new model, simulation of flex was instrumental to the goal of reducing weight without loss in strength or rigidity. A base cover that used carbon fiber reinforced plastic (CFRP) with an aluminum shield would offer support to the motherboard. The LCD screen would be protected by a rear cover with CFRP and graphite-fiber reinforced plastic (GFRP).

Analysts simulated the physical tests that were performed on a magnesium LCD frame, an LCD panel assembly, a rear cover made of PC/ABS, and a CFRP base cover with its aluminum shield in place. "We applied loads of 400 to 3200 grams, and we compared the resulting deformation to physical test results," says Dr. Xin. "In each case, simulation had a close correlation with real-world behavior during physical testing."

In a whole machine analysis, engineers evaluated the performance of laying-up composite CFRP for the rear cover; this kind of composite material could enhance much of the strength for the entire machine. "In this instance," Dr. Xin says, "the nonlinear capabilities of Abaqus were valuable to us because of the complex performance properties of the materials, complex geometry deformation and complex contact behavior." Engineers also evaluated two alternatives for the array of CFRP: horizontally versus vertically orienting the fibers. The analysis found that horizontal lay-up of the fibers resulted in smaller deformation. The engineers were also able to prove out the strength of a (now-patented) joint line for combining CFRP and GFRP. Due to composite CFRP being limited by part geometry shape, the rear cover is made of both CFRP and GFRP through the patented joint method.

Analysis weighs alternatives

The Kodachi (ThinkPad X300) project proved that the simulation tool has the ability to provide accurate results, allowing engineers to predict the strength of the structure and offer suggestions to CAD designers, on the project codenamed Shinai (ThinkPad T400s), for example. Analyzing deformation of the closed notebooks under a press load revealed that the Light Emitting Display (LED) stress was much lower than in the Kodachi design. During press load on the rear cover of the whole machine, the Kodachi LED contacted the track-point—the cursor tracking button in the ThinkPad keyboard—potentially creating as much as 8.4 MPa of stress. By contrast, the LED on the Shinai contacted the palm rest on the base, yielding a much lower stress of 2.2 MPa.
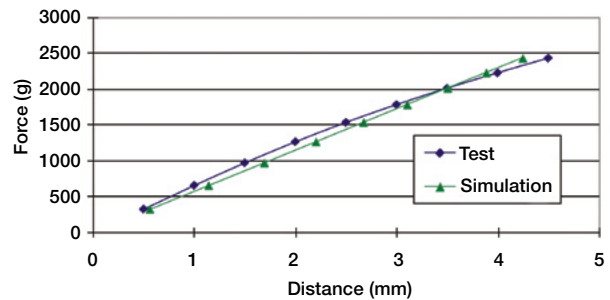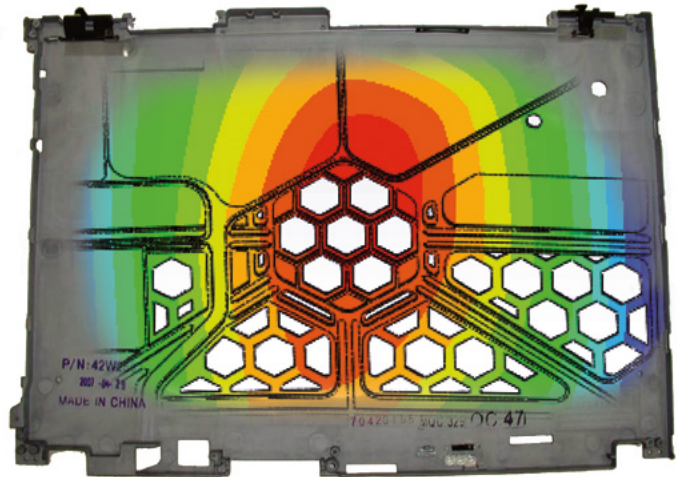
Abaqus FEA simulation of a Lenovo ThinkPad magnesium frame (above). Test and simulation correlation, Lenovo ThinkPad magnesium frame (right).

The analyses also showed that four areas on the magnesium frame of the Kodachi design exceeded specifications for material yield strength and created deformation of the rear cover of 5.8 mm, resulting in higher overall deformation than on the Shinai, which only exceeded specs of material yield strength in one area. The data from the simulation guided revisions to the Shinai frame, helping the development team speed up the project schedule. "Because of our work with Abaqus," Dr. Xin says, "we were able to fix the Shinai design quickly and easily." In both cases, FEA results were quite similar to physical test results.

FEA gets in touch with keystroke feel

Keyboard design is a strong selling point for the ThinkPad. The notebooks have long been known for their sturdiness and their pleasing signature "feel"—the physical response of keys being pressed. In the case of a new keyboard, the engineers wanted to reduce the thickness of the assembly (thereby making the overall notebook slimmer) but still keep their traditional keystroke feel.

Source: SIMULIA Community News, September 2011

"'Feel' may sound like a vague term," Dr. Xin says, "but with FEA, it is actually quantifiable." To confirm that the feel remained the same from the old keyboard to the new, engineers simulated the effects of keystroke pressure on the original dome-shaped rubber spring, the central component that provides each key with its resistance and spring-back. Because the rubber dome was axisymmetric, they were able to model a 2D half-section of the spring and run the analysis on that. The nonlinear simulation enabled the engineers to establish values—on a feeling chart—for how far the rubber dome traveled downward (compressed) as keystroke force increased. (Typical typing force is between 0.6 to 1.2 Newtons.)

The engineers then used Abaqus to evaluate a new rubber dome design for the thinner keyboard in order to match the keystroke behavior of the old rubber dome. "The feeling chart of the new simulation showed close correlation with the old one," Dr. Xin says, "and both simulations matched up well with data from physical testing."

These are just some of the simulations a Lenovo ThinkPad undergoes on its way from design to reality. The motherboard itself is also analyzed (and physically tested) for flex, and the Ball Grid Array (BGA) components are modeled undergoing strain to confirm that the solder joints will perform well. "As always, nothing validates a simulation like its close conformity to real-world testing," Dr. Xin notes. "The push-point tests of the motherboard, and the strain tests for the BGA, were based closely on our physical prototype testing, and they yielded similar results."

All of the simulations at the Lenovo IDC yield the same result: high-performance, quality products that undergo less prototyping, reach production faster at a smaller cost, and perform reliably for users, from museum curators to coffee-fueled college students.

Automated framework to estimate probability of mechanical failure in handheld electronic devices

Manish Maheshwari, Alberto Cavallaro (Motorola Mobility LLC – a Lenovo company)

Abstract: An automated framework for numerical simulation is developed to estimate the probability of brittle failure for a cell-phone display subjected to accelerated life cycle testing (ALT). SIMULIA Isight and the Abaqus-Python interface are used to predict the field-failure rate (FFR). The framework's adaptable definition of inputs and output parameters can be extended to other common failures in handheld devices such as the denting and cracking of the housing walls, the cracking and delamination of the solder-joints in surface mounted devices, and the shock based criteria for packaged components.

Keywords: statistical probability, field-failure-rate, FFR, accelerated-life-cycle test, ALT, consumer electronics, cell-phones, LCD, OLED, display, brittle failure, Isight, Python, automation, statistics

1. Introduction

Electronic device manufacturers necessitate predicting the field-failure-rate for the life of a product to compute warranty costs. Accelerated life-cycle testing of prototypes is often used to estimate the field-failure rate and entails a sequence of tests that represent everyday use and abuse, such as dropping, scratching, bending, environmental exposure, and thermal cycling. However, the drive to reduce design cycle-time and to use fewer prototypes can result in uncertainty around these estimates. Fortunately, advancements in finite element analysis allow us to simulate most of these mechanical test cases and, with a statistical consideration for the ALT sequence, are used to estimate the FFR.

A significant shortcoming to this numerical approach is the amount of time spent by the engineer to set-up the numerous load cases as well as to post-process the large amount of output data. This study demonstrates the use of Isight and the Abaqus-Python scripting interface to significantly reduce pre and post-processing time. The inherent capabilities of Isight include tools such as design-of-experiments, survival distribution, response-surface analysis, and Monte-Carlo simulation, which facilitate defining the load conditions and sequence, as well as analyzing the output response.

This paper describes the overall framework and applies it to predicting display failure for a mobile which undergoes accelerated life-cycle testing. The framework is designed with flexibility in defining the input and output parameters so the same approach can be extended for virtually any other failure mode in the system.

2. Automated Framework:

The high-level flow for the full framework (Figure 1) entails the following steps: calculating the statistical distribution of the failure strength for the component or material of interest; defining and running the simulations for the load-cases to generate the response surface models for the resulting stresses in the component and material of interest; and finally run a MonteCarlo interference analysis of the imposed stress and failure strength yielding the FFR of the component or material.
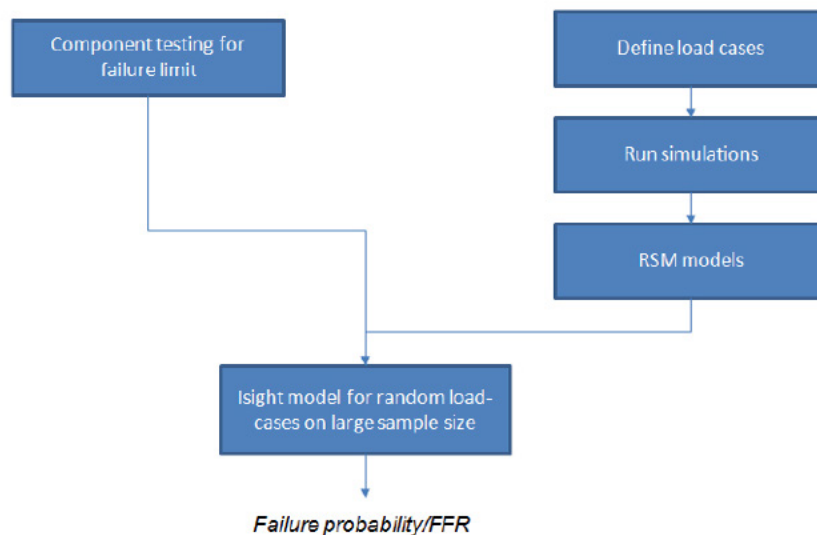

Figure-1: High level flowchart for the framework

Source: Science in the Age of Experience Conference, 2016

The following sections highlight the step-by-step approach used to build a generic framework for predicting failures in a given component and is divided into 5 major steps. Some suggestions are included as well to yield superior accuracy from the numerical models and an example is built around modeling display failures in a mobile phone exposed to drop.

2.a.   Component/material failure limit: Most material/components exhibit unit to unit variation in the failure limit for a given failure mode. Component level testing of a statistically significant sample size that exhibits the same failure mode is used to parameterize the statistical distribution of the failure strength.

Minitab or any other statistical tools, is initially used to estimate the minimum sample size. In this particular example (Figure 2) assuming a normal distribution, a 90% confidence level (e.g. 0.1 margin of error) and a standard deviation of 0.2 requires 13 units for our test. We later elect to use 20 units.
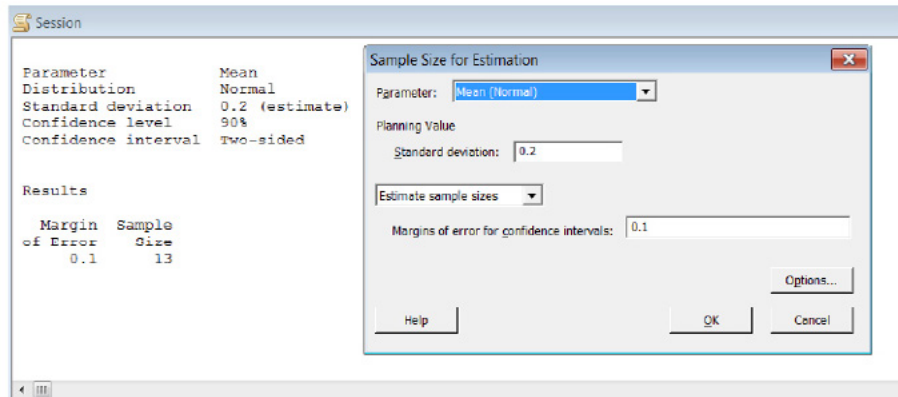

Figure2: Estimate sample size for probability estimate for given failure mode using Minitab software

4-point bend testing is conducted on 20 samples to extract the strength distribution for the glass in a display (Figure-3). The parameterization of the data with a Weibull fit yields the input parameters for the framework used later in steps 2-c and 2-d.
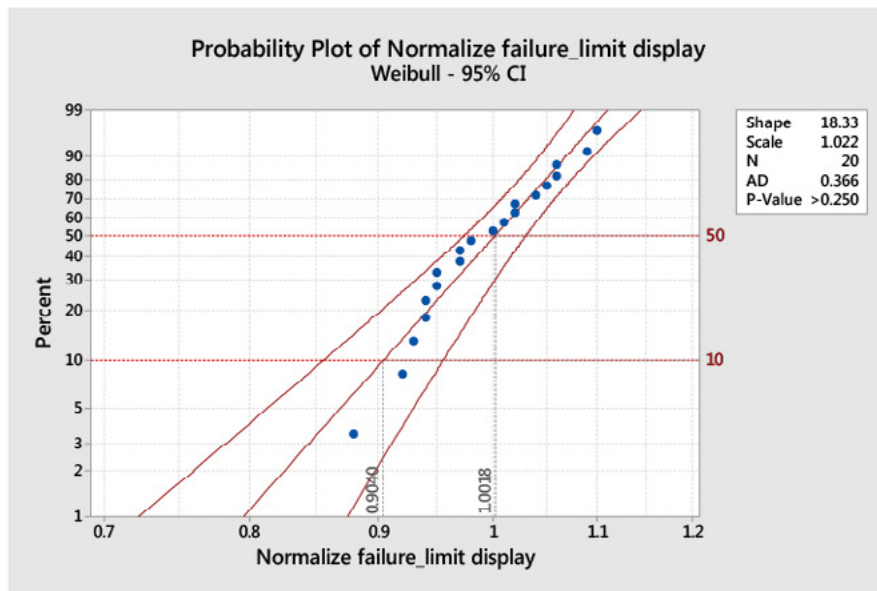

Figure-3: probability plot showing the statistical distribution of normalized failure limit for tested samples

Source: Science in the Age of Experience Conference, 2016

2.b.   Define Load cases: The load case is defined by the mechanical load and boundary conditions on the component or material. The best suited problems for the framework are the one where loads and boundary condition can be parameterized.

For a display, more than 90% of mechanical failures had been associated with system drop from a certain height. The stress on the display glass obviously varies with drop-height and drop-orientation, which can defined by rotation angle in roll and pitch direction from base orientation (Figure-4). Therefore we have three input parameters to define a load case:

i)   Height

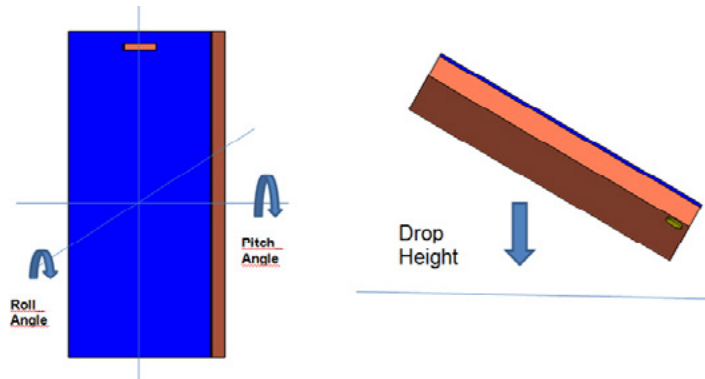ii)   Roll_angle

iii)   Pitch_angle

Figure-4: Load case for phone drop model

When a phone is dropped accidentally by the end-user, the above parameters will be random and uniformly distributed over certain bounds,   However, during accelerated life testing in a lab, the release drop angles are targeted to particular orientations (say face, back, side or corner drops) to simplify the test sequence and insure that most regions of interest are evaluated. This procedure yields a higher frequency of impacts close to targeted angles.

To mimic the lab scenario the distribution of drop angles and height is weighted creating a distribution for specific conditions that more likely occur in the controlled accelerated life test (Figure-5). This distribution is fitted from experimental characterization of 60+ drops for 3 phones which was recorded and analyzed with a high speed camera. This distribution becomes the input function for our framework as described in steps 2.c and 2.d.
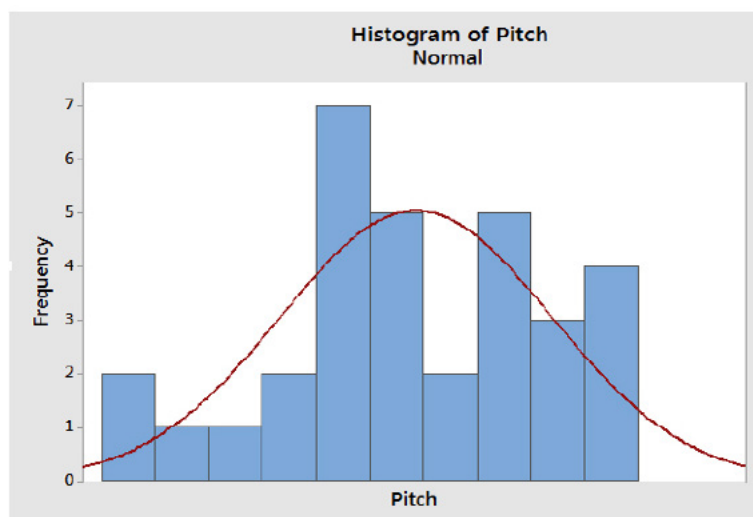

Figure-5: Distribution of pitch_angle when dropped from various heights

2.c. Run Drop simulations: By defining bottom drop as the zero-angle, the pitch and roll angles of -180° to +180° represent all of the possible drop orientations. We use a DOE and response-surface-model to predict stress values for any random orientation in this space.

The Isight Sim-flow (Figure-6) generates the simulation load-cases, creates the input files, runs the simulation jobs, reads the results, and saves them into a data file. The data file will be later used to create the response-surface-model.
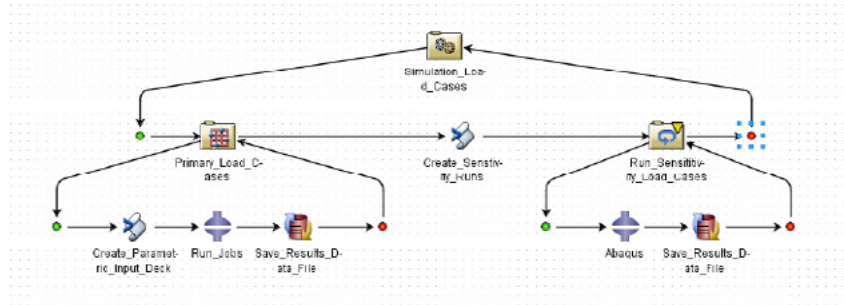

Figure-6: Isight Sim-flow showing framework to automatically generate load-cases and submit the simulation jobs on cluster

Furthermore, the functions used of this flow entail the following:

i) DOE: It generates 50 random drop angles and heights within the specified bounds. Optionally a latin-hypercube approach can be used in this specific case but any other approach with sufficient number of cases will also work.

Tip: If part of design space is safe for a given problem – that it can be skipped and results can be made zero or lower than the failure limit using calculator function without running the simulation jobs to save time.

ii) Create_parametric_input_Deck: A python script is used to read the DOE parameters as input for the orientation and height, and to modify the template for the simulation input deck. Here, the drop angles and height are specified as the parameters for the drop simulation model. These parameters will be used to rotate the model with *NCOPY command.

****

*PARAMETER

*PITCH_ANGLE = <pitch_angle_from_script>

*ROLL_ANGLE = <roll_angle_from_script>

*DROP_HEIGHT = <drop_height_from_script>

****

iii) Run_Jobs: The Abaqus function in Isight reads the input deck created by the script, runs the simulation jobs, and reads the peak stress on the display from simulation output database (*.odb) file.

Tip: We use the simulation grid engine to submit jobs for this display problem since the simulation jobs are very complex and run for a long time. The python script creates the input decks in Isight while another script that runs when the job is complete on the simulation grid engine generates the results.

The display strain is written as part of the history output with the"ANTIALIASING" filter and at a 20 kHz frequency. The peak strain is read using the python script on a pre-specified set and then stored in the data file against the matching load case.

***

*OUTPUT, HISTORY, FILTER=ANTIALIASING, TIME INTERVAL=0.005

*ELEMENT OUTPUT, ELSET=DISPLAY-GLASS

LEP2, LEP1, LE11, LE22

***

iv) Data exchanger: The cata exchanger function writes the results in text file in the CSV (comma separated values) format where first three columns write the pitch_angle, roll_angle and height and the fourth column writes the peak strain data for display (Figure-7)

```
Pitch_Angle, Roll_Angle, height, Peak Strain
60.8,    -45.2,  3.2,    0.98
-121.3, 176.2,  4.8,    0.67
22.4,    -2.0,  5.0,    0.39
105.1,  26.4,  2.7,    1.67
```

Figure-7: Results stored in CSV text file

v) Script_Create_Sensitivity_Runs: Another python script reads the results from the data file and compares the stress/strain value against nominal failure limit. If the maximum stress/strain value is >30% of the nominal failure value, it creates an additional 2 to 4 simulation jobs around that orientation to capture the sensitivity in pitch and roll directions.

The sensitivity runs shows how fast the high stress/strain changes when we change the drop angle by few degrees around a high stress condition.

The script creates the input decks for sensitivity runs and updates the loop parameter to adjust additional jobs that might be needed.

vi) Loop function: It funs all the sensitivity runs by reading the input deck and appending the results into the results file.

2.d. Response-surface-model: For this display problem, we run between 200 to 300 simulations at various drop angles, drop heights and sensitivity angles around the high-risk orientations. The results are then stored in the data file in CSV format.

Tip: Most RSM models try to minimize error over the whole design space and this practice can often average and thus ignore highly localized peak values. Based on our experience we have divided our design space in multiple segments (4 in this display problem) to get higher accuracy for each of the smaller design spaces.

Steps:

i) The Isight Approximation function is used to create the response-surface-model.

ii) The RBF model is best suited for display problems since there are localized peaks at specific angles.

iii) The results data file is used as an input to the Approximation function.

iv) The "Dynamic file" is used as the data input file so that the program can update the input file as more simulation jobs complete in the background. Therefore, the final results are up-to-date with the current data.

v) The elliptical basis function is best suited to minimize the error in display problem but this is very specific to type of runs and should be verified for each new program and data

vi) Cross-validation is used for error analysis accepting an RMS error less than 10% for the model.

In Figure-8 the RSM model is shown for a smaller design space around a high stress area: the red color envelopes the high risk region.
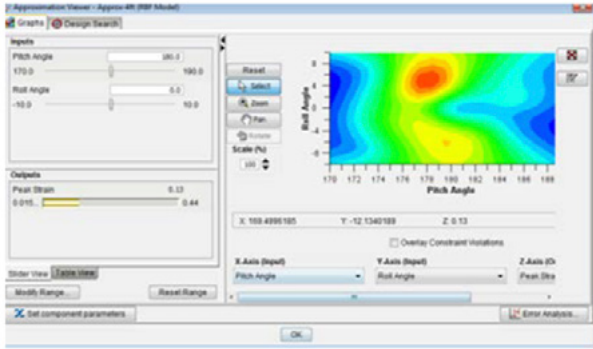

Figure-8: one of the RSM model showing hotspot near high risk simulation

Source: Science in the Age of Experience Conference, 2016

2.e. Estimate probability of failure: Once we have the response-surface-model to predict the simulation results for all parameters, we can run the Monte-Carlo simulation to create a large number of load-cases without running each finite-element simulation.

Tip: The model accuracy is highly dependent upon number of simulations run over design space and using FMEA or experience to capture most of the high risk orientation in design-space.

A model is built around the actual accelerated-life-cycle test (ALT). The test sequence is replicated into Isight using Monte-Carlo simulation, RSM and standard math operations. Figure-9 shows the flow-chart for a generic ALT and Figure-10 shows the flow-chart for an Isight model that runs the ALT with ntotal number of units.

While the general ALT includes a sequence of mechanical, thermal and environmental loads, we focus on the mechanical loads as they are the ones that apply to the anticipated display failures. Using simulation data and the Isight model, we can run the sequence of load-cases on several hundred or several thousand units instead of the 20 to 30 units used during physical testing. Steps in modeling the ALT flow to calculate probability of display failures follow.

i) ALT loop is defined using MonteCarlo loop with input parameters as pitch_angle, roll_angle and height. The distribution for each parameter is defined using weibull distribution captured from testing.

ii) ntotal units are number of units used that goes through sequence of load cases.

iii) For each unit, a Monte-Carlo loop will randomly select failure limit from the Weibull distribution captured in step 2.c

iv) For each load-case (defined by randomly selected pitch, roll angles and height), we calculate the peak-stress from the response-surface-model associated with that load-case

v) The peak-stress is now compared against the failure limit to decide whether the unit survived load-case or not. If survived it is subjected to next load case

vi) If the failure is defined as accumulated damage then the damage_parameter is updated at the end of each load

vii) Once the unit has been through all the load-cases, we can assess pass/fail/total-damage for the unit.

viii) The process is repeated for each unit and we count the total number of failure units nfail

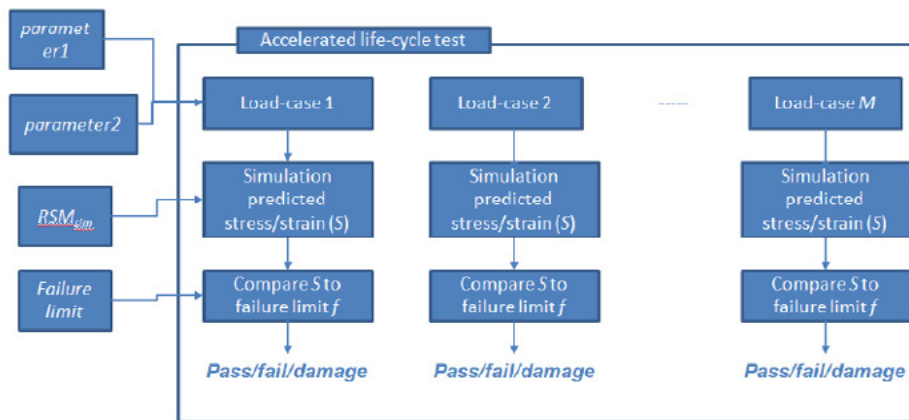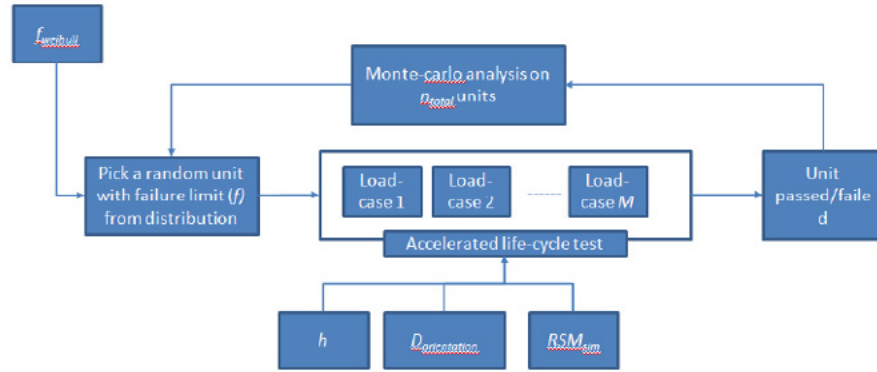ix) Probability of failure of a given component is the ratio nfail / ntotal

Figure-9: Flow-chart showing accelerated-life-cycle-test case model

If n_{fail} units failed from n_{total} units, then probability of failure P_{fail} is:

$$P_{fail} = n_{fail} / n_{total}$$

Figure-10: Monte-Carlo simulation model to assess probability of failures on large number of units

Figure-11 shows the snapshot from the I-sight model showing 2 Monte-Carlo loops. The outer loop picks a random unit with a failure limit from the Weibul distribution. The nested inner loop runs the ALT for a random load-case and captures if unit passed/failed.
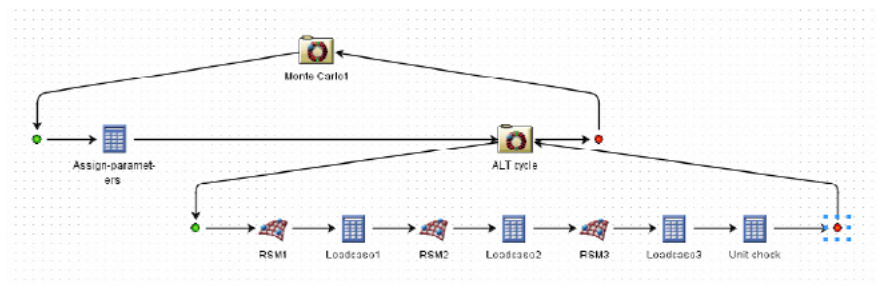

Figure-11: Isight model snapshot for probability of failure calculation

3. Extensions of the study

3.a. Calculate Field-Failure-Rate: While the lab testing for prototypes generally have predefined sequence of loads and targeted height and orientations for drop testing, in the real-world the loads and orientations are random.

As we used a normal distribution for pitch_angle, roll_angle and height about specific orientations and heights for ALT, we can change the distribution to uniform to predict the actual field-failures which are random about the orientation. If we employ a large number of units (i.e. 10,000 for the display failure example) in the analysis, we can quantify the related field-failure rate.

3.b. Ductile failures: Section-2 was heavily focused on brittle failures in display. However, the Isight model is flexible to define ductile failure or damage to component as well. In section 2.e we can use the peak-stress/strain to calculate total damage to the material/component. Or the damage model can be defined into an Abaqus-material model and we can read the damage variable instead of peak-stress and move down the sequence of loads to capture total damage to the component.

Source: Science in the Age of Experience Conference, 2016

4. Advantages and limitation of the approach

4.a. Averaging in response-surface model: Most response-surface models or statistics tend to ignore/average the outliers to get accuracy in maximum design space of input parameters. Take the example of a random drop for a hand-held device. In the continuous space of roll and pitch angles from -180° to 180°, only few orientations may result in failure for a given height and most of the design space may remain safe. If we try to capture the whole continuous space in one RSM model, the model may totally miss the high risk zone(s). Therefore selectively dividing the RSM model in multiple spaces using FMEA or past experience gives us choice to look at the broader orientations without missing local peaks.

4.b. Damage to other components is ignored in sequence of load cycle: since we are focusing on one-component during our study here, we are ignoring damage to other components and assembly during the sequence of load cycles. Several times, the damage to other components may lead to higher probability of failure in our component of interest. Based upon heuristic models, additional correction in stress/strain can be added to the sequence of loads address this issue.

4.c. Validation: Receiving FFR (field failure rates) data from field is challenging unless we warranty the product for given failure. Therefore our model focused on validating a total of 4 products with 100+ sample size as physically tested in our lab. When a good correlation was found with these products, we were able to build confidence that the FFR data should be accurate for field and start using that to assess warranty cost.

5. Summary

This study demonstrates the capability of an automated numerical framework to predict the probability of brittle failure in a display during a targeted load cases like ALT for predicting field failure rates. The approach is generic and can be used for modeling most mechanical failure including but not limited to brittle failure of glass and ceramics as well as defining the damage accumulation in ductile materials. Like most numerical models, the design is sensitive to the numerical inputs, and the number of simulation jobs run to build the RSM models. Very precise steps should be taken leveraging the experience form past failure modes when defining these parameters.

Trademarks:

1) Isight and Abaqus are trademarks of Dassault Systèmes Simulia Corp.

2) Minitab is a trademark of Minitab Inc.

Acknowledgement

This work was performed at the Motorola Mobility LLC laboratories

Disclaimer

This communication may contain information and data that has been normalized. Any opinions or information expressed regarding 3rd party products or services do not constitute an endorsement from Motorola Mobility LLC. Neither Motorola Mobility nor the Author shall be liable for any unauthorized use, or amendment, or the consequences thereof.

Source: Science in the Age of Experience Conference, 2016

Estimating Acoustic Performance of a Cell Phone Speaker Using Abaqus

C. Jackman and M. Zampino (Foxconn Holdings LLC)
D. Cadge, R. Dravida, V. Katiyar, J. Lewis (DS SIMULIA)

Abstract: Consumers demand smaller electronics devices with more features and capabilities. Making devices smaller provides challenges to engineers to maintain the acoustic performances as enclosed acoustic volume sizes are reduced. This paper discusses the requirements for coupled structural-acoustic simulation and demonstrates the application of this technology to cell-phone acoustic design. Due to the smaller volume sizes, the low frequency response of the cell phone is affected. The frequency response rolls off faster at low frequencies when smaller microphone back volumes are used. The present work deals with studying this effect on a simple cell phone model with the finite element package, Abaqus. The results from the simulation can be used in better designing cell phone cavities for optimum performance.

Keywords: Diaphragm, Acoustics, Impedance Boundary, Topology, Merge/Cut, Tie, Back Volume

1. Introduction

Cell phone industry has been making great advances in terms of packing more features while reducing the size of the instrument itself. As the size reduces, it presents more challenges to the overall acoustic performance of the cell phone. At low frequencies, the acoustic pressure emitted by a cell phone device is affected by the size of the back volume which in turn is affected by the size of the instrument. Hence, in order to improve the acoustic performance cell phone designers often use more than one speaker. Additionally, the size of the back volume that would give the optimum acoustic performance has to be prototyped and developed. Fortunately the availability of finite element software codes, such as Abaqus, avoids the time consuming and expensive process of building and rebuilding of back volumes to physically test the optimum performance.

Abaqus's general nonlinear mechanics capabilities have been used for twist, hyperextension and drop test simulations (Nagaraj, 2002; Thiruppukuzhi, 2008; Theman, 2005). The general mechanics capabilities clubbed with the coupled structural-acoustic capabilities make Abaqus a powerful tool to solve the most important problems related to the cell phone industry. Powerful Abaqus/CAE modeling capabilities (including easy import of geometry from third party CAD software, a wide variety of meshing tools, virtual topology etc) along with a number of structural, acoustic element types and a broad range of material models make Abaqus a versatile software for these kinds of simulations. Additional features include nonconforming tie between structural and acoustic elements, and availability of a variety of acoustic output variables. In the present work, we setup a dual-speaker model in Abaqus and compare the simulation results of the acoustic pressure at a certain distance in the exterior of the diaphragm when the speakers are excited by a mechanical force.

2. Physics of the problem

The geometry of the speaker is shown in the Figure 1. The diaphragm (yellow) is excited due to the rocking motion of the voice coil. By driving a current through the voice coil, a magnetic field is produced. This magnetic field causes the voice coil to react to the magnetic field from a permanent magnet fixed to the speaker's frame (Figure 1), thereby moving the diaphragm. A detailed plot of the diaphragm is shown in Figure 2. It can be seen that the annulus region of the diaphragm has corrugations. The corrugations are employed in most of the commercialized mobile speakers to enhance the high-frequency sensitivities to the required levels. In this way, a fairly flat frequency response over a broad range can be achieved to avoid sound distortion to human ears. Accurate modeling of such a response can be achieved only through a detailed finite element simulation. Other techniques such as the lumped parameter (Beranek, 1954; Small 1972; Small 1972) approach may not yield accurate results at high frequencies.
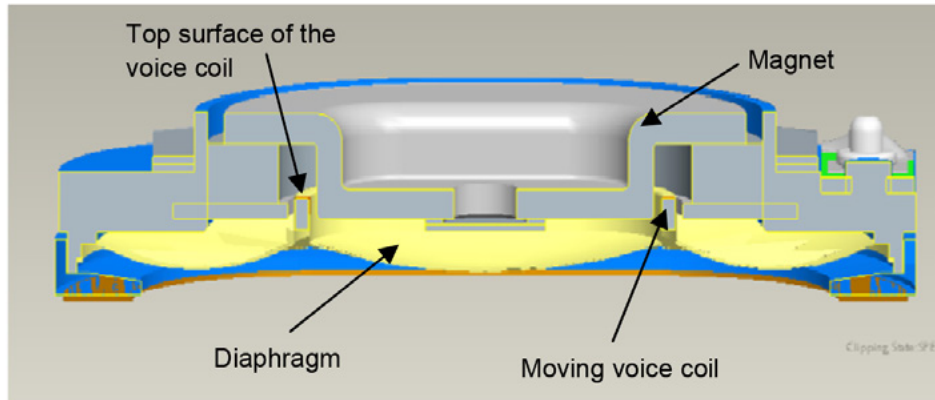
Figure 1. Geometry of the speaker used in the present work.

As the size of the cell phone decreases, the volume of air behind the diaphragm becomes smaller. This small amount of volume behind the speaker limits the range of motion of the diaphragm. The speaker does not produce enough force to compress the air beyond a certain point, hence causing the air to push back. This reduces the displacement of the speaker diaphragm, which in turn lowers the output. The frequencies affected the most by this are the ones with the largest amount of displacement, (low frequencies). This effect can be modeled in Abaqus using acoustic elements, which have predefined bulk properties to capture such volumetric effects automatically.
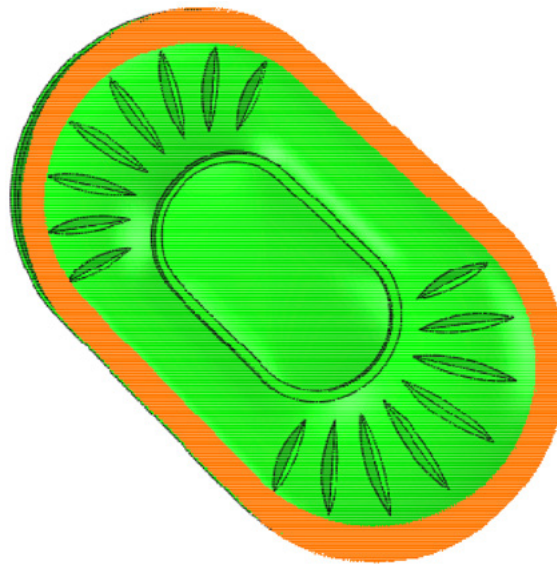

Figure 2. Diaphragm.

The function of the vents (shown in Figure 3) is to ensure that the diaphragm does not undergo static deformation due to changes in the atmospheric pressure while the back volume is maintained at a constant pressure when it is sealed. The static deformation would not only cause damage to the diaphragm but also can alter its acoustic performance. One disadvantage of the vent is that it excites an undesirable resonant peak called the Helmholtz resonance (Pierce, 1989), which may occur in the audio frequency range. When the diaphragm vibrates, part of its displacement compresses air inside the back volume and the remainder moves air outward through the vents. The mass of air displaced through the vent (acoustic mass) in combination with the stiffness (air in an enclosed volume tends to get compressed due an excitation) offered due to the air in the back volume produces the Helmholtz resonance. In order to tune this peak to acceptable levels, the speaker manufacturers apply a netted material on the vent.
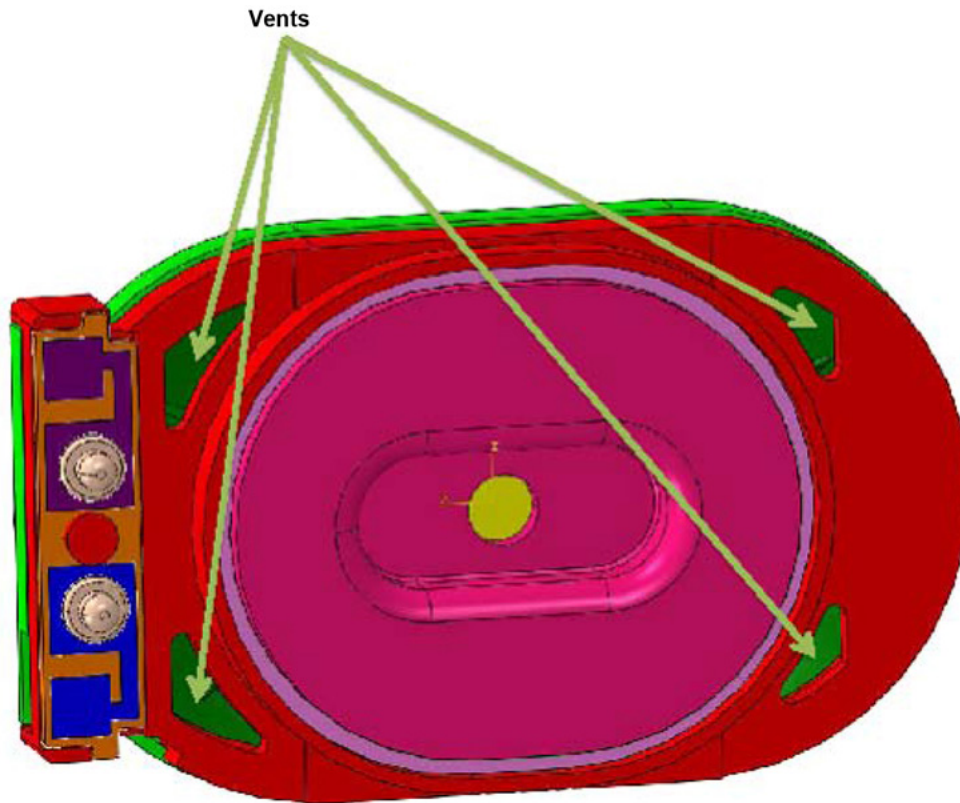
Figure 3. Bottom view of the speaker geometry showing the vents.

3. Model Setup

We have taken two approaches to run the simulations. One is to replace the convoluted membrane with a planar membrane and tune the material properties (Young's modulus and density) and thickness of the membrane materials. The method relies on experimental data for two cases; case 1, when the speaker's back volume is enclosed such that the volume of air contained in it is 2cc and case 2, when the speaker's front and back volumes are separated such that there is no acoustic interaction between them (this condition is referred to as an infinite baffle in the literature). The thickness and density of the voice coil and the diaphragm are tuned such that the simulation results match the experimental results of both cases. The results obtained by performing simulations with the tuned parameters have to be compared with another measurement with a different back volume. This is a work in progress as we will be comparing the tuned results with a 3.5 cc back volume case.

The second approach is to model the actual dual-speaker geometry in Abaqus. This methodology is advantageous because the physics of the problem is captured accurately without the need for any approximations. Also since we are using the actual geometry and the material properties, the laborious tuning methodology employed in the first approach can be completely avoided.

The original CAD speaker model was imported into Abaqus/CAE. Abaqus/CAE is a CAD neutral system, and is designed to be able to import and use geometry from many third party proprietary CAD systems, as well as neutral file formats. In some cases parts or part instances contain details such as very small faces and edges. These features, although important for machining and packaging of a component, have little impact on the mechanics of the problem. Including such features in the numerical analysis may lead to very fine mesh density leading to increased computation times. The virtual topology feature in Abaqus/CAE allowed us to exclude such small details by combining the feature with an adjacent larger feature. Nodes and elements are still created to conform to the original geometry.

Boolean operation in assembly module of Abaqus/CAE was utilized to cut out the speaker geometry from the acoustic domain (Further details about virtual topology and Boolean operation can be obtained from Abaqus/CAE user's manual). The

"cut" operation leaves holes in the acoustic domain for regions which will be filled later with the speaker geometry to create the complete system. The assembly of acoustic front and back volumes is shown in Figure 4. The diaphragm occupies the region in between the front and speaker's back volumes. The other speaker components which hold the diaphragm in place were considered rigid and so were not modeled, and boundary conditions were not applied to the acoustic regions that are in contact with the surfaces of these components to enforce this rigid assumption (In Abaqus acoustic domain without any boundary condition assumes a rigid termination).
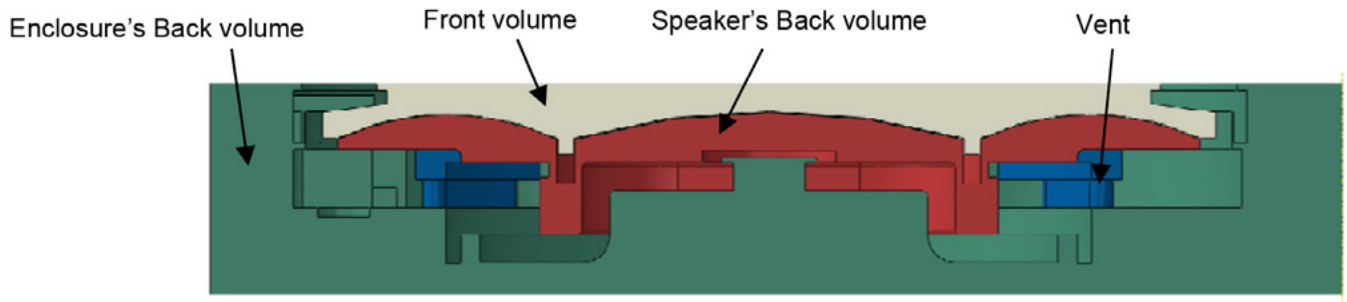

Figure 4. Speaker diaphragm assembled with front and back volumes of the acoustic domain. The green (dark) portions represent the acoustic domain. Grey (light) portion represents the diaphragm and the moving coil. The void region represents the rigid components of the speaker.

3.1 Elements, Boundary Conditions, Loads and Domain Size:

The diaphragm is modeled with modified three-dimensional solid elements (Abaqus keyword *ELEMENT, TYPE=C3D10M) and was assigned the physical properties for the material of the diaphragm given as per the manufacturer's specifications. Modeling the diaphragm with solid elements (instead of shell elements) allowed us to cut away the acoustic domain more easily. The acoustic domain, both in the back volume and the volume exterior to the diaphragm, is modeled with three-dimensional acoustic elements (*ELEMENT, TYPE=AC3D4). These elements were assigned the physical properties of air. For problems that include unbounded acoustic domain, a boundary condition has to be applied at the exterior boundary to minimize reflections. This can be achieved by applying nonreflecting surface impedance boundary conditions (*SIMPEDANCE, TYPE=SPHERICAL) to the exterior mesh as shown in Figure 5. A pinned boundary condition was applied on the outer surface of the diaphragm (red or dark region in Figure 2) which in the actual speaker geometry was sandwiched between two bodies.

The accuracy of an acoustic analysis depends on two factors: element size in the acoustic domain and the overall size of the exterior domain. It is recommended that at least six representative inter nodal intervals fit into the shortest wavelength present in the analysis. Generally, if greater accuracy is desired 8 to 10 elements per wavelength should be used. If the domain size is many wavelengths at least 15 elements per wavelength have to be used to counter numerical dispersion. The numerical dispersion is the decay in acoustic pressure as a function of distance solely due to accumulation of numerical errors from one element to the next, which is a result of having fewer elements per wavelength (Figure 5 has an illustration of finite element mesh considerations for an acoustic analysis). In the present work, eight elements per wavelength were chosen to run the analysis. It is recommended that the domain size is at least 1/3rd of the longest wavelength (lowest frequency present in the analysis). This number, although arbitrary, ensures that the reflections from the far field are minimized when the acoustic boundary is terminated with nonreflecting impedance boundary conditions.

As the frequency range of interest grows the size of the model may approach the upper limit of memory and disk space on the computer. Hence, it is advisable to split the analysis into multiple runs with smaller frequency ranges of interest. In the present analysis our frequency range of interest from 200 Hz to 5000 Hz is split into two analyses; one from 200 Hz to 1000 Hz (Low frequency analysis) and the other from 1000 Hz to 5000 Hz (High frequency analysis).

Non-reflecting boundaries

Radius of domain corresponds to one-third of the longest wavelength

Element size corresponds to one-eighth of the shortest wavelength
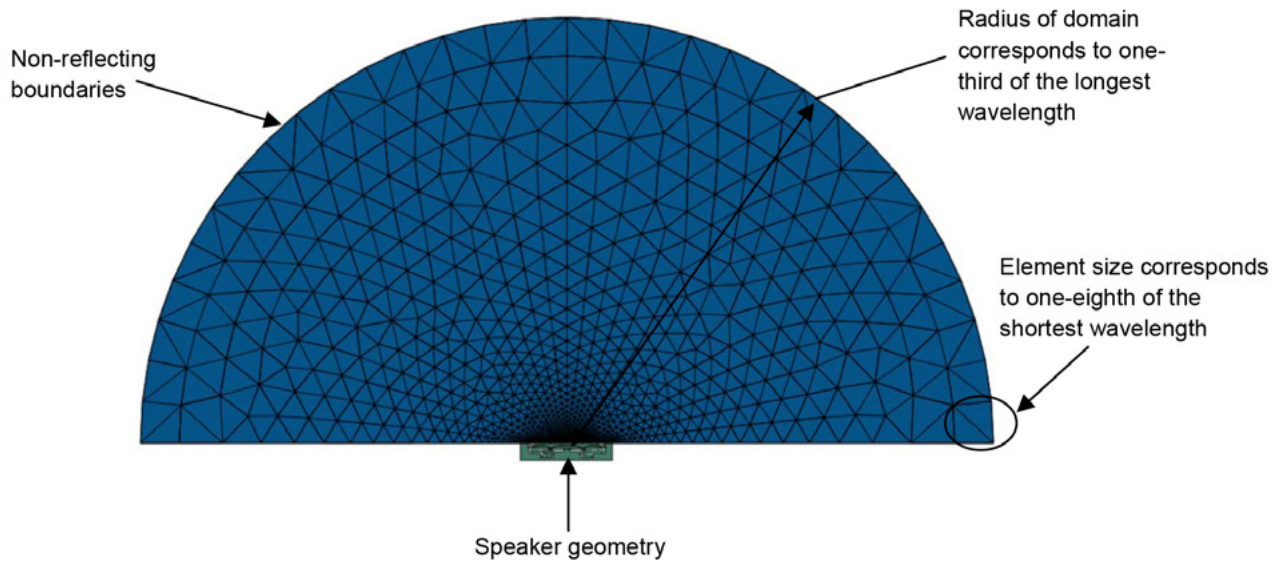
Speaker geometry

Figure 5. Mesh properties for the acoustic domain driven by a single speaker.

To provide coupling between the structural and the acoustic domains, tie constraints (*TIE) were applied between the acoustic medium and the front/back surfaces of the speaker diaphragm. Non-conformal tie constraints are used by Abaqus to provide a structural acoustic coupling without creating Acoustic Structural Interface (ASI) elements. This makes model setup simple whilst provides the necessary coupling between the acoustic and structural domains of the problem.

A direct-solution steady state dynamic analysis (*STEADY STATE DYNAMICS, DIRECT) was used to run the analysis. This procedure conducts a frequency sweep by applying the loading at a series of frequencies and extracting the magnitude and phase response of the system (Refer to Abaqus Analysis User's Manual). A load (*CLOAD) of unit magnitude (constant value at all frequencies) was applied to the top surface of the voice coil (see Figure 1) in both the low frequency and high frequency analyses.

4. Analysis Methodology

The mass of the voice coil (see Figure 1) is the only unknown in the model as it depends on the length and density of the coil wire and had to be chosen, by trial and error, to ensure that the resonant frequency matches the manufacturer's specifications. Tuning the mass of the voice coil required us to run a direct-solution steady state dynamics analysis (from 200Hz to 1000Hz) on the diaphragm, without the acoustic domain, in the presence of high enough damping in order to obtain the displacement response at the center of the diaphragm. The damping of the diaphragm (*STRUCTURAL DAMPING) was chosen such that the quality factor (Pierce, 1989; Thiel, 1972) at the resonant peak matches with the manufacturer's specification. Additional damping was added to account for the electrical effects. The effect of the magnetic field, length of copper wire used to create the electro-magnet, as well as the resistance of this copper wire, is to create a resistance in series with the structural damping resistance provided by the diaphragm (See paper by Thiel: "Loudspeakers in Vented Boxes: Part-1" Figure 3), and the applied excitation load is scaled independent of frequency. This means that the effect of the electro-magnetic parts of the system is to add damping to the system (Thiel, 1972).

At the end of this process, the actual displacement may not match the experimental measurements but the general shape of the curve will align. This is because of using an approximate unit load as the forcing function. The physical forcing function on the diaphragm cannot be calculated in Abaqus as it is based on electrical excitation (If the electrical circuit is simple enough to be approximated by a lumped parameter model, it may be possible to calculate the equivalent mechanical components and run the complete electro-mechanical analysis in Abaqus. The static characteristics of the electromagnetic driver and its effect on the mechanical displacement of the diaphragm can be obtained by creating a user element) and hence the loading has to be approximated. It is also assumed that the force (as a function of frequency) is independent of the size of the back volume. Since the diaphragm displacement and the subsequent acoustic response are considered to be linear phenomena, the results

Source: SIMULIA Community Conference, 2009

can be scaled after the analysis to match the measurements. The following paragraph details the scaling procedure.

The analysis is performed assuming a unit load on the top surface of the voice coil (see Figure 1) and a calibration vector, which is a linear ratio of the acoustic pressure measured to the acoustic pressure from the Abaqus results as a function of frequency, is calculated. This calibration vector can be multiplied with the acoustic pressure results from subsequent analyses (with different back volumes), provided that unit excitation is applied on the diaphragm in those cases as well.

5. Acoustic pressure and displacement calculations

The acoustic pressure in the exterior domain at a distance of 10 cm away is shown in Figure 6. The mechanical force applied on the diaphragm (due to the electrical excitation) was not known and so an arbitrary value of 1 unit load was chosen to run the Abaqus simulation. Hence, the results in Figure 6 do not match but the general shape of the curves is identical. The calibration vector, shown in Figure 7, is the ratio of Abaqus response (due to unit excitation) to the measurement.
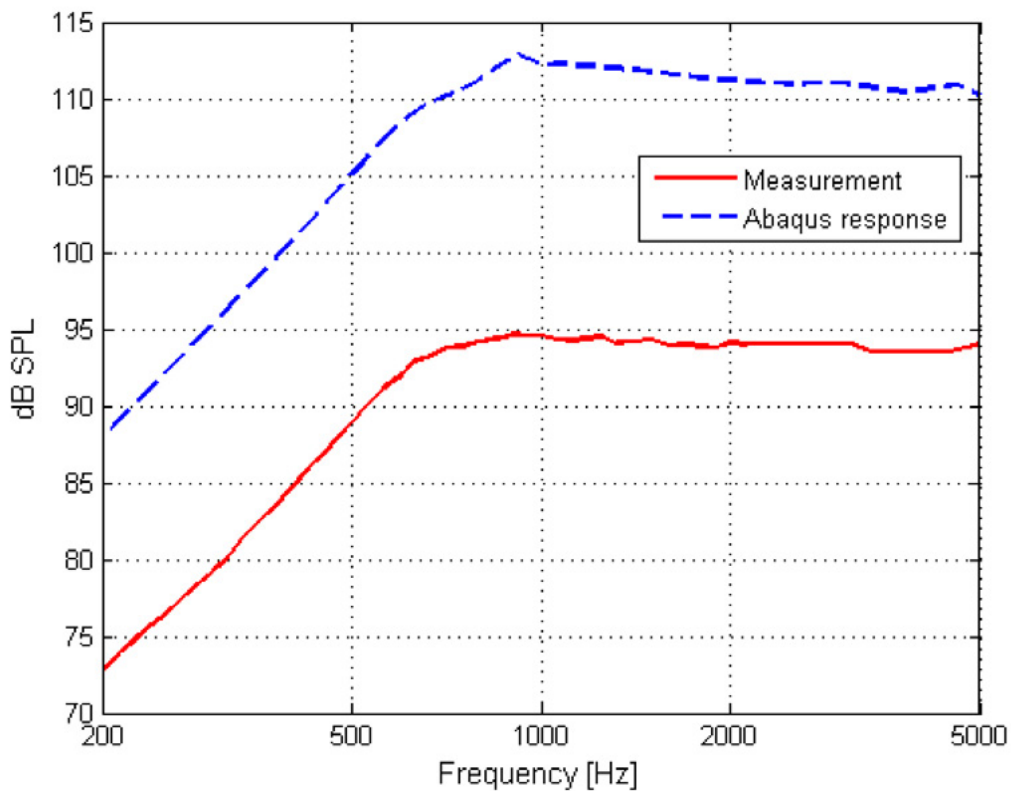

Figure 6. Comparison of Abaqus response with the measurements performed by "Manufacturer B". An arbitrary excitation load of one unit was chosen in the Abaqus analysis as the excitation due to electrical load was not known and hence the results do not match.
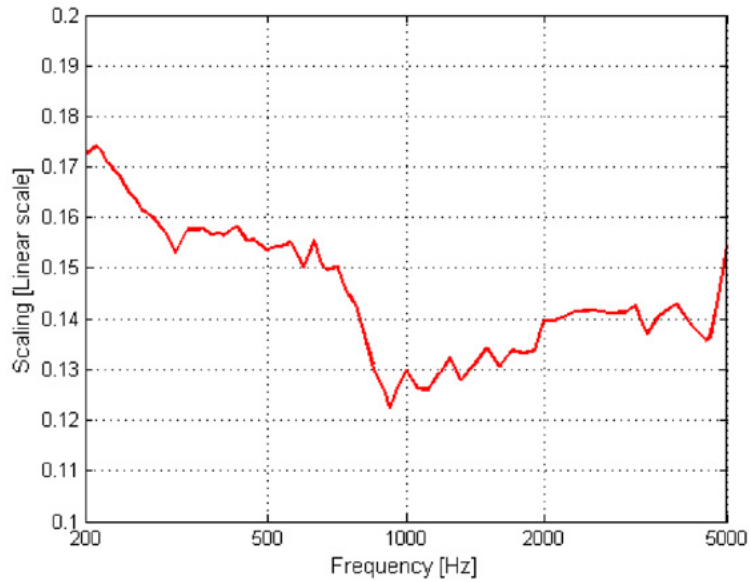
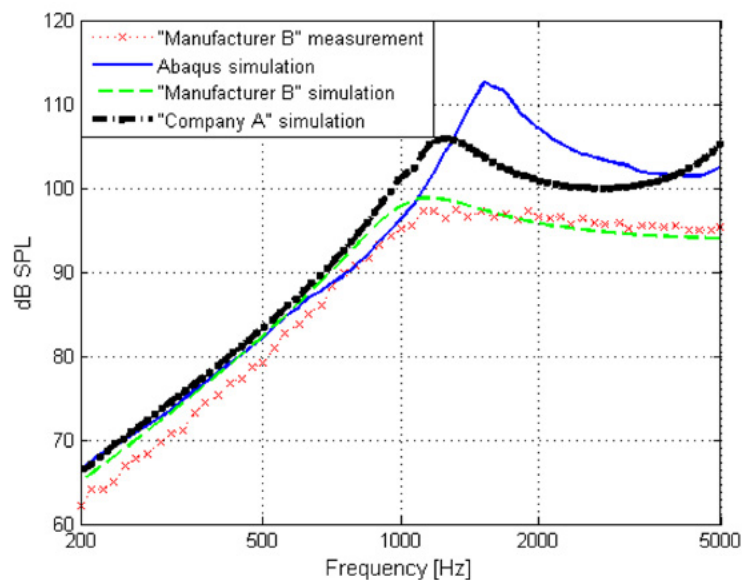Figure 7. Calibration vector computed by taking the ratio of measured to Abaqus responses from Figure 6.

Figure 8. Comparison of results when the speaker was enclosed in a 2cc back volume.

In Figure 8 the results of Abaqus analysis have been compared with simulation results from a mobile device company (labeled in Figure 8 as "Company A"), a speaker manufacturer (labeled in Figure 8 as "Manufacturer B") and measurements from the latter. The "Company A" results have been obtained by approximating the system as lumped parameters (effectively reducing the whole system into electrical equivalents). It can be seen that the low frequency analysis results of Abaqus simulation matches well with the other simulation results and reasonably well with the measurements. The Helmholtz resonance peak at 1500 Hz, in Abaqus and "Company A" simulations, is due to the interaction of vent holes (acoustic mass) with the 2cc back volume (acoustic compliance). The reason for suppression of the peak in "Manufacturer B" results is unknown at this time; we are in the process of obtaining this information.

6. Conclusions

The present work shows that acoustic analysis in Abaqus can capture a) Helmholtz resonance and b) the reduction in acoustic pressure at low frequencies due to the presence of back volume. These effects play an important role in choosing the appropriate back-volume size during a cell phone design and in choosing the appropriate vent size during the speaker design.

The results of Abaqus simulations have been compared to those from a mobile device company and a speaker manufacturer. The results below 1000 Hz agree very well between the three simulations and the measurement. The Helmholtz resonance peak that exists in Abaqus, "Company A" results is not seen in "Manufacturer B" results and the subsequent higher frequencies are also affected by the resonant peak. The reason for this discrepancy is being investigated.

7. Future work

Several improvements can be made to the modeling strategy to reduce the analysis time.

Infinite elements can be employed instead of the nonreflecting impedance boundary conditions. The domain size required for infinite elements to work effectively is much smaller than the size required for nonreflecting boundaries. The infinite element formulation has a ninth-order truncation of the reflections, where as the nonreflecting boundaries have a zero-order approximation.

Use mode-based steady state dynamics (*STEADY STATE DYNAMICS, SUBSPACE) instead of the direct solution (*STEADY STATE DYNAMICS, DIRECT).

Model the diaphragm with shell elements instead of solid elements. This will reduce additional computation time associated with solving equations of the solid elements.

8. References

1. Beranek, L. L., "Noise and vibration control", McGraw-Hill, New York, 1954.

2. Nagaraj, B., Motorola, "Two Step Method of Analyzing Hyperextension Problems with Large Contact Interactions Using ABAQUS/Explicit," ABAQUS Users' Conference, pp. 1 – 7, Newport, Rhode Island, May 2002.

3. Pierce, A. D., "Acoustics: An Introduction to Physical Principles and Applications", Acoustical Society of America, pp. 121, 330, 1989.

4. Small, R. H, "Direct-Radiator Loudspeaker System Analysis", Journal of Audio Engineering Society, Vol. 20, Num. 5, pp. 383-395, June 1972.

5. Small, R. H., "Closed-box loudspeaker systems-part 1: analysis" J Audio Eng Soc, Vol. 20, Num. 10, pp.798–808, 1972.

6. Theman, M., and Poskiparta, P., Nokia, "Evolution of Mobile Phone Drop Test Simulation at Nokia," ABAQUS Users' Conference, pp. 1 – 1, Stockholm, Sweden, May 2005.

7. Thiel, A. N, "Loudspeakers in Vented Boxes: Part I", Journal of Audio Engineering Society, Vol. 19, Num. 5, pp. 382-391, May 1971.

8. Thiel, A. N, "Loudspeakers in Vented Boxes: Part II", Journal of Audio Engineering Society, Vol. 19, Num. 6, pp. 471-483, June 1971.

9. Thiruppukuzhi, S., Motorola," Probabilistic Simulation Applications in Product Design," Abaqus Users' Conference, pp. 285 – 301, Newport, Rhode Island, May 2008.

Lowest Cost Printer Chassis Design that Would Pass a Series of Transportation Drop Tests, Utilizing Design of Experiments in Conjunction with Abaqus/Explicit Analysis

Amin Godil (Xerox Corporation, Wilsonville, Oregon)

Abstract: A printer chassis provides an important function of locating and securing the relative position of all the sub-systems that makeup a printer. The customer location could be thousands of miles away from the factory and many modes of transportation are required from ship, train, trucks, forklift, to pushing across corridors, stairs and elevators. The transportation loads are the most sever the printer would see in its life time. These include impacts on all sides at 3 MPH to an 8 inch vertical drop. In today's competitive market cost is as critical a function as performance to succeed in the market. To design the lowest cost chassis, 3 large highly stressed parts in the chassis were optimized for cost. Two parameters; sheet metal thickness, and material strength were used to minimize the chassis cost provided the combination passed each one of the six unique transportation tests. A six factor, two levels, Taguchi L12 matrix was utilized for the design of experiment (DOE). Abaqus/ Explicit analysis were used for virtual transportation testing to compute the output responses of the DOE. The design optimization exercise resulted in an addition 6% cost savings.

Keywords: Abaqus/Explicit, Abaqus/CAE, Chassis, Cost, Design of Experiments, Drop Test, Finite Element Analysis, Impact, Mild Steel, Noryl, Optimization, Plastic Strain, Printer, SECC, Structure, Simulation, Taguchi L12, Transportation Test, Welding, Wood

1. Introduction

A printer chassis is the backbone of the printer. Its function is to provide support and location to all of its subsystems, customer user interfaces like screens and keyboard but it also has to protect its content from abuse and damage during the life of the printer. The propensity and severity of damage is the largest during its transit from the factory to customer locations thousands of miles away. All modes of transportation are realized by the chassis during its life from fork lifting, truck ride, train haul, freight container across the oceans and pushing across the hallways to its final destination at the customer site. For the chassis to be robust against failures from vertical drops to accidental bumps on all of its sides and edges, a series of transportation tests have been defined for new design qualification.

2. Transportation Test

The transportation testing specifications is an internal Xerox document that defines a suite of tests both packaged and unpackaged. The testing is comprised of handling tests that require the product or package be dropped from different heights depending on product weight. The product or package has to be dropped on its bottom and also roll dropped on its four edges and four corners. Three miles per hour impact on all of its four sides and a random vibration test to a predefined power spectral density is also required. Table 1.0 summarizes the entire tests that were required for the particular chassis design.

Abaqus/Explicit was used to simulate the entire test suites defined in Table 1. Most of the chassis members were sized based on stress feedback from the simulations.

3. Chassis Design

The design is sized based on the constraints from the various subsystems and customer requirements. The chassis weight is determined by the subsystem mass added to the chassis structure. A typical office printer would weigh between 300-500 lbs and the picture of a typical printer and its chassis are shown respectfully in Figure 1., and Figure 2.

The chassis structural members are all constructed from electro galvanized sheet metal that is cut and bent into shape. The members are assembled together by a combination of methods that include, welding (TIG, MIG, Spot, Laser) and fastening, the methods selected are to minimize the overall assembly cost.

Source: SIMULIA Community Conference, 2011

Table 1. Transportation tests considered for the particular product chassis

Test	Packaged	Unpackaged
Free Fall Height (inch)		
-Bottom	8.0	2.0
-Sides	6.0	2.0
-Corners	6.0	2.0
Incline Impact Speed = 3MPH		
-All Four Sides	Yes	No
Obstruction Crossing Speed = 3MPH		
-Barrier Height (inch)	No	0.5
-Gap Height x Width (inch)	No	2.0 x 1.75

Figure 1. Xerox Office Printer ColorQube 9303

Figure 2. Printer Chassis

Source: SIMULIA Community Conference, 2011

The preliminary sheet metal thickness of the chassis members was done by hand calculations. The chassis was design using Wildfire 3.0 and was subsequently imported into Abaqus/CAE. Most of the sheet metal was already near the desirable 1.0 - 1.2 mm thickness. Three major structural components, base, mid-rails and vertical columns were still at the higher 2.0 mm thickness and were therefore selected for optimization, see Table 2.

Table 2. Chassis member's thickness and parts selected for design of experiments

Part Description	Quantity	Thickness (mm)	Thickness Change
Base	1	2.0	Design of Experiment
Lower Shear Panel	1	1.2	NO
Rear Left Side Column	1	2.0	Design of Experiment
Scanner Support beam	1	1.2	NO
Scanner Support Panel	1	1.2	NO
EB Rear Bracket	1	2.0	NO
EB Front Bracket	1	2.0	NO
Torque Tube	1	1.6	NO
Mid-Rail	2	2.0	Design of Experiment
Mid Panel	1	1.0	NO
Top Rear Rail	1	1.2	NO
Tray Left	1	1.2	NO
Tray Right	1	1.2	NO
Tray Support	1	1.2	NO
Back Panel	1	1.0	NO
Front Left Side Column	3	2.0	Design of Experiment
Right Shear Panel	1	1.2	NO
Display Panel	1	1.0	NO
Scanner Side Bracket	1	1.0	NO
PP Vertical	1	1.0	NO

4. Material Properties

The material used for the chassis structural parts was commercial grade Steel, electro galvanized cold rolled (SECC). Most of the chassis was made out of SECC and for higher strength SECC390 was considered. The true stress strain cure for both metals is presented in Figure 3. The entire chassis was modeled with three basic material, wood for the shipping pallet, mild steel for the all of the metal parts and Noryl 4025 for the plastic parts that included the castor wheels. The mechanical properties of the material are presented in Table 3.

Table 3. Material properties used for simulation

Material	E (MPa)	Density (Kg tonne/mm³)	Poissons	Yield Strength (MPa)
Mild Steel	2.07E+05	7.80E-09	0.29	206
Noryl 4025	9.00E+03	1.43E-09	0.3	
Wood	3.73E+03	5.00E-10	0.3	

Source: SIMULIA Community Conference, 2011

4.1 Design Allowable

Only a small percentage of printers in the field are subjected to the extreme drop and impact conditions and therefore an aggressive design allowable of 3.0% was used as the acceptable maximum equivalent plastic strain in any of the structural members. Provided the total plastic strain does not result in excessive permanent deformation that would cause any catastrophic failures, long term performance issues, are visually not detectable and are outside the customer field of view.

5. Design of Experiment

Three structural parts shown in Table 2, above were used and both material strength and thickness were varied at two levels, this resulted in a six factor two level DOE. Taguchi L12 DOE matrix was used for regression analysis as shown in Table 4.

The costs for each run were calculated from vendor data and were plugged into the DOE matrix in Table 4. All twelve simulations were run using Abaqus/Explicit which took approximately ninety hours. All simulations except the first one meet all of the structural design allowable requirements as define in section 4.1. Run 2 results in the lowest cost printer chassis about 6% lower than the baseline design without the optimization.
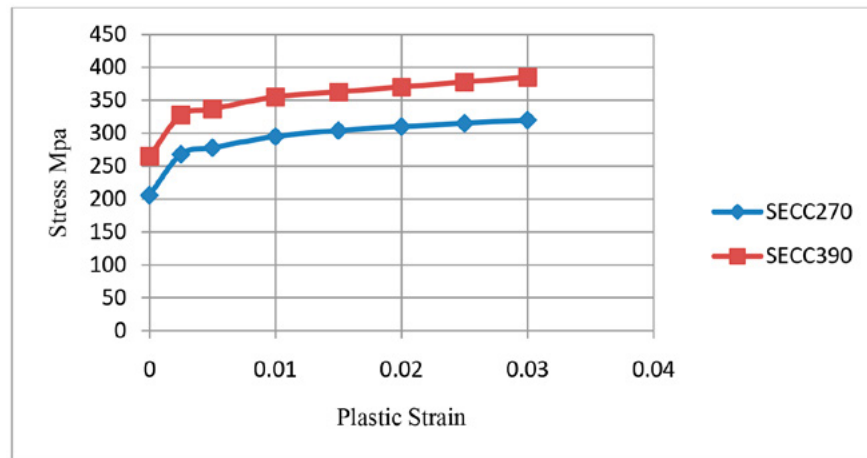

Figure 3. True Stress-Strain Plot

Table 4. Taguchi L12 DOE matrix with cost response

Factor	A	B	C	D	E	F	Cost($)
Row #	BeamT	BeamS	ColumnT	ColumnS	BaseT	BaseS	Y1
1	1.6	270	1.6	270	1.6	270	72.143
2	1.6	270	1.6	270	1.6	390	73.524
3	1.6	270	2	390	2	270	77.75021
4	1.6	390	1.6	390	2	270	75.668
5	1.6	390	2	270	2	390	78.48123
6	1.6	390	2	390	1.6	390	77.17021
7	2	270	2	390	1.6	270	76.02121
8	2	270	2	270	2	390	78.71323
9	2	270	1.6	390	2	390	77.61323
10	2	390	2	270	1.6	270	75.10858
11	2	390	1.6	390	1.6	390	75.38958
12	2	390	1.6	270	2	270	75.25758

6. Simulation Results

The simulations were done on a Dell Precision T7500 work station with two Intel Quad core Xeon processors each running at 2.2 GHz. Abaqus 6.10 running on Windows 7, with a 64 bit operating system was used. A typical output plot of von Mises stresses of the entire chassis is shown in Figure 4.
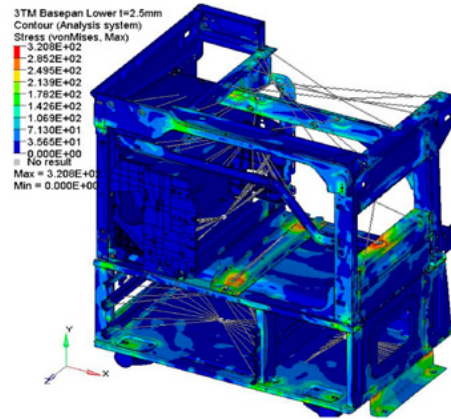

Figure 4. Typical chassis drop simulation results, von Mises Stress

The model contained about 200,000 elements and it required about 7.5 hours for each drop simulation run. The simulations were done utilizing Abaqus/Explicit and were used to screen out the DOE designs shown in Table 4. that did not meet the design allowable requirements as defined in section 4.1. All of the simulation except the first run passed the allowable test.

There were some interesting observations for the simulation runs a few are presented below;

Internal energy absorbed by various members of the chassis structure is shown in Figure 5. The wood pallet absorbs about 30% of the internal energy followed by 15% for the base pan and the rest is absorbed by the remaining components.

The thinner higher strength material base pan absorbs about 19% more internal energy than the thicker lower strength counterpart, see Figure 5.

The impact loads on the castors is about 8% lower with the thinner higher strength base pan compared to the thicker lower strength base pan, see Figure 6.
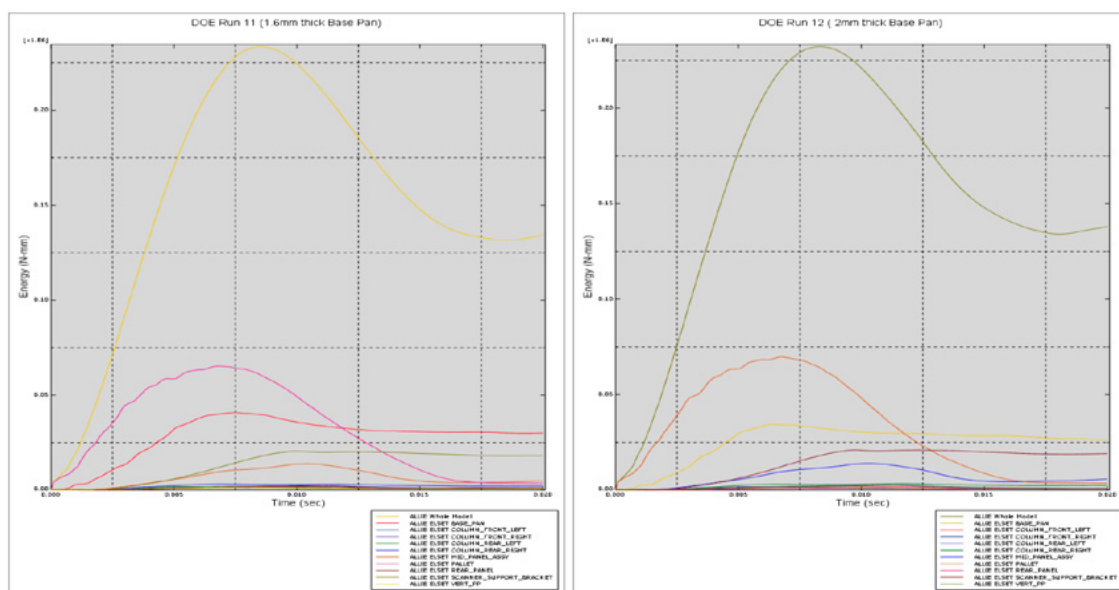

Figure 5. Internal energies of structural members, Base Pans 1.6mm (left), 2mm (right)

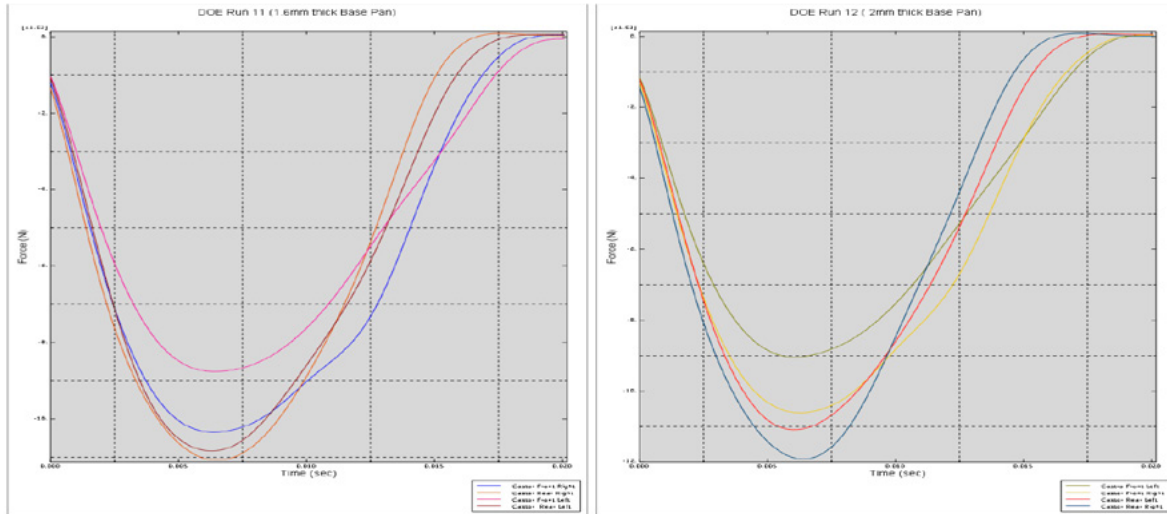Source: SIMULIA Community Conference, 2011

Figure 6. Loads on all four castors, Base Pans 1.6mm (left), 2mm (right)

6.1 Internal Loads

Internal loads both force and moments between major structural members were recorded during all of the simulations and then the peak loads were used to design the welded joints, see Table 5.

Table 5. Internal loads and moments

Interface	Side	Force (N)			Moment (N-M)		
		F1	F2	F3	M1	M2	M3
Column/Base	Front-Left	467.0	-2704.0	-395.0	-65.2	16.6	46.8
	Front-Right	402.0	-2618.0	-713.0	-62.0	16.4	-57.0
	Rear-Left	90.0	4207.0	1178.0	190.0	23.0	1.0
	Rear-Right	257.0	4720.0	1262.0	228.0	-2.6	31.0
Mid Rails/Column	Front-Left	2049.0	6015.0	1260.0	-24.0	32.0	90.0
	Front-Right	4114.0	3245.0	1878.0	32.0	-12.0	24.0
	Rear-Left	676.0	3616.0	313.0	-51.0	12.0	44.0
	Rear-Right	3178.0	5207.0	-1065.0	-25.0	-17.0	13.0

7. Conclusions and Next Steps

The chassis design was optimized for cost using design of experiments in conjunction with Abaqus /Explicit to validate the design robustness to transportation requirements. This strategy resulted in an additional 6% cost savings on top of the already cost reduced chassis design. The entire cost optimization exercise was conducted virtually; no actual parts were available for testing. This provided us with a head start in the design cycle and now the parts will be released with higher level of confidence. The aggressive design allowable requirements set for the chassis would have not been possible without detailed finite element analysis simulating the drop and impact of the chassis.

The next step is to build real parts and assemble them into an operational chassis and verify the results of the simulation. If there are no large surprises then the virtual optimization of the chassis would be a great success story in terms of design schedule and cost optimization.

8. References

1. Abaqus/Explicit: Advanced Topics, Lecture Notes
2. Xerox internal transportation specifications document
3. Xerox internal material data sheets

Source: SIMULIA Community Conference, 2011

Temperature Cycling Analysis of Lead-Free Solder Joints in Electronic Packaging

Shan Li*, Zhenyu Huang and Jianfeng Wang (Intel (Shanghai) Technology Development Ltd., Shanghai, China)
Shaowu Gao (Abaqus Shanghai Office, Shanghai, China)

Abstract: Numerical simulations have found growing interests in evaluating interconnect reliability in electronic packaging, particularly for lead-free solder joints. To achieve good predictive capability, appropriate constitutive properties for the solder balls and a damage mechanism based life prediction model must be provided. In this paper, a simple published but efficient approach is adopted to predict life of SnAgCu joints subjected to temperature cycling. Specifically, the constitutive properties of the solder joints are described by the ABAQUS built-in Anand model, and the energy based Darveaux model is used to predict the fatigue life. The complete finite element model and its analysis are done in ABAQUS using its scripting interface. Finally a numerical example is presented to illustrate the procedures, and, hence, demonstrates the capability of ABAQUS in electronic packaging modeling.

1. Introduction

Solder joints have been widely used in the ball grid array (BGA) package to provide electrical and mechanical connections between the package and the PCB Board (see Fig. 1). However, a major concern with the solder joints is the effect of temperature cycling on the reliability of electronic packages since they are mainly subjected to cyclic power and thermal loadings during their service life. As the coefficients of thermal expansion (CTE) of the materials used in these packages are drastically different (2~3 ppm for die and 40~60 ppm for molding compound and die film), temperature variations create thermal mismatch resulting in solder joint stress during heating and cooling cycles. The damage caused by these stresses accumulates as the electronic assembly is subjected to thermal cycling, eventually leading to fatigue failures of solder joints. Thus, measuring thermal fatigue life of solder joint has always been an important factor when evaluating a package for a particular application.
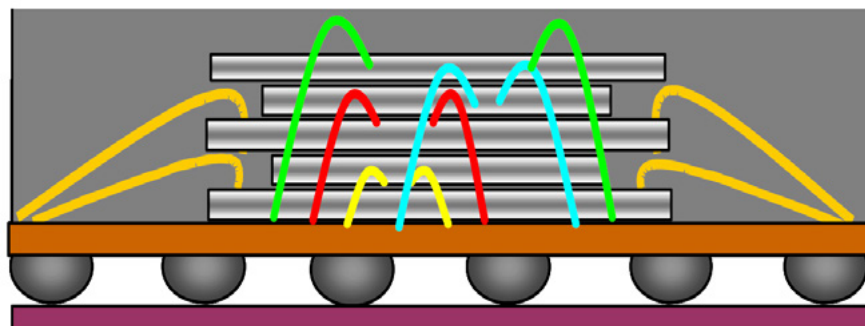

Fig.1 Schematic drawing of a ball grid array package

Traditionally, the thermal fatigue life of solder joints is measured by performing temperature cycling tests which may take up to months. Even with accelerated life tests adopted, the task still remains formidable. With the maturity of numerical techniques and sophistication of computer resources, numerical simulations have rendered it possible to predict the life of solder joints without resorting to lengthy and costly tests. Compared with tests, numerical simulations are much cheaper and faster and can be readily used to aid designers in assessing risk at the early stage. Because of the benefits, now IC companies rely heavily on numerical simulation for reliability assessment of solder joints. However, to achieve good predictive capability, appropriate constitutive properties for the solder balls and a damage mechanism based life prediction model must be provided. Over the past decades, a number of models have been proposed to study lead- and lead free solder joints. Lau and Rice [1990] adopted an empirical elasto-plastic stress-strain relation for solder alloys. Wiese et al [2003] identified two mechanisms for steady state creep deformation of Sn4.0Ag0.5Cu (SAC405) solder and adopted a double power law to simulate climb controlled (low stress) and combined glide/climb (high stress) behavior. Darveaux [2000] used Anand visco-plasticity model

Source: Abaqus User Conference, 2007

Contents

[1985, 1989] to describe solder joints behavior at high temperatures and decomposed the failure into crack initiation and crack growth, both of which were approximated by power law.

The purpose of this work is to develop a modeling tool for new product thermal fatigue risk assessment as compared with old products benchmark values, therefore focus will be on aiming at "relative" life prediction rather than "absolute" values. The Anand Visco-plasticity model, which has been implemented in ABAQUS as a secondary creep law, is used in this study. Also since Darveaux's damage model [2000] has been verified by several researchers within 25% prediction accuracy, the previously published Data for both crack initiation and propagation are adopted to predict the thermal fatigue life for the lead-free sold joints. The complete finite element model and its analysis are done in ABAQUS using its scripting interfaces and global / local analysis technique is used to enhance the computation efficiency.

2. Constitutive properties

For most of metal alloys, creep usually occurs when homologous temperature, defined as the ratio of absolute temperature to the absolute melting temperature, is larger than 0.5. Since the melting temperatures of solder are around 200°C, time-dependent creep phenomena are expected to dominate solder joint fatigue even at room temperature.

As shown in Fig. 2, creep deformation can be roughly divided into three regions:

Region I - Primary creep, which has a rapid rate initially and slows with time;

Region II - Secondary creep, which has a approximately uniform rate;

Region III - Tertiary creep, which has an accelerating creep rate and terminates by failure of material at time for rupture.
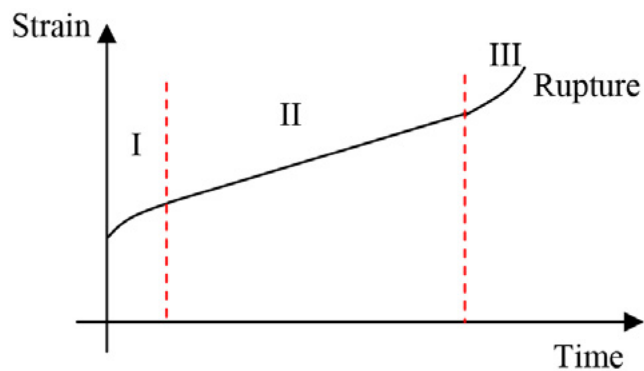

Fig.2 Strain Vs. Time Creep Behavior

In semi-conduct industries, the deformation kinetics of solder alloys is dominated by the steady state creep deformation due to their low melting point. Therefore, only the steady state creep behavior is considered in this study. The Anand model [1985, 1989], a viscoplasticity model that combines plasticity and creep deformation, is chosen to represent the secondary creep of solders. For ABAQUS Version 6.6, the Anand model is provided in the form of a built-in user material.

In Anand's model, the secondary creep is described by a flow equation:

$$\frac{d\varepsilon_p}{dt} = A\left[\sinh(\frac{\xi\sigma}{s})\right]^{\frac{1}{m}} \exp(\frac{-Q}{kT}) \tag{1}$$

where Q is the activation energy, k is the Boltzmann's constant, T is the absolute temperature, s is the flow stress, A is the pre-exponential factor, m is the strain rate sensitivity, x is the multiplier of stress, and s is the deformation resistance stress built-in as a state variable and its evolution is given by the following three equations:

$$\frac{ds}{dt} = \left[h_0 (|B|)^a \frac{B}{|B|} \right] \frac{d\varepsilon_p}{dt} \tag{2}$$

$$B = 1 - \frac{s}{s^*} \tag{3}$$

$$s^* = \hat{s} \left[\frac{1}{A} \frac{d\varepsilon_p}{dt} \exp\left(\frac{Q}{kT}\right) \right]^n \tag{4}$$

where h0 is the hardening/softening constant, a is the strain rate sensitivity of hardening, $\hat{S}$ is a coefficient for deformation resistance saturation value, and n is the strain rate sensitivity for the saturation value. As can be seen in the above equations, there are nine material parameters in Anand model: A, Q, x, m, h0, $\hat{S}$, n, a, and s0

(initial value of the deformation resistance). The values for Sn4Ag0.5Cu (SAC405) solder are tabulated in Table 1[Reinikainen et al, 2005].

Table 1. Anand's constants for SAC405 solder [Reinikainen et al, 2005]

Parameter	s_o (MPa)	Q/k (K)	A (1/sec)	ξ	M	ho (MPa)	$\hat{S}$	n	a
Value	1.3	9000	500	7.1	0.3	5900	39.4	0.03	1.4

3. Life prediction models

To predict the fatigue life of the solder ball, a sophisticated model that incorporates damage should be provided. Among all of the strain and energy based methods, Darveaux's model is arguably the most popular one due to its documented correlation with the actual tests. In Darveaux's model [Darveaux, 2000], the failure can be split into two parts: the life associated with crack initiation and the life associated with crack growth. The number of cycles before crack initiation is given by:

$$N_0 = K_1 \Delta W^{K_2} \tag{5}$$

And the crack growth rate per cycle is given by:

$$\frac{da}{dN} = K_3 \Delta W^{K_4} \tag{6}$$

Where DW is inelastic energy density accumulated in a cycle, Ki (i=1..4) are material constants of the particular sold joints. Assuming uniform crack growth rate during crack propagation, the total cycles before failure are the summation of two failure mechanism:

$$N_a = N_0 + \frac{a}{da/dN} \tag{7}$$

where a is the total distance the crack has to propagate until completed separating the solder joint from the board or the package. Here it can be assumed as the diameters of the interfaces near the package side or the board side. As observed in

Source: Abaqus User Conference, 2007

tests (see Fig. 3, Ghaffarian, 2000), thermal fatigue failures usually occur at the interfaces near either package side or board side. Therefore, a can be assumed as the solder diameters of the package-side or board-side interfaces.
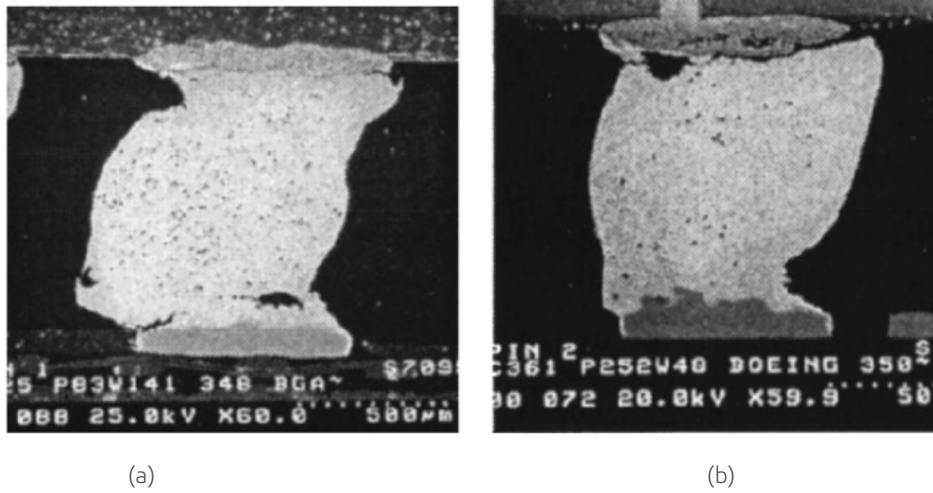

(a)   (b)

Fig. 3 Common failure modes in thermal cycling tests (Ghaffarian, 2000)

The values for Ki for SAC405 joints are directly quoted from Darveaux [2000] and listed in Table 2.

Table 2. Darveaux' life prediction constants for SAC405 solder [Darveaux, 2000]

Parameter	K_1 (cycles/MPa^{K_2})	K_2	K_3 (mm/cycles/MPa^{K_4})	K_4
Value	11.6	-1.52	7.71×10^{-9}	0.98

4. Finite element implementation

To obtain the mechanical responses of the solder balls under thermal cycling, finite element code ABAQUS 6.6 [ABAQUS 6.6 manual] is used to perform the analysis. Because of the large number of solder balls involved in a package and severe nonlinearity of Anand model, a single-step analysis of the full package with PCB board attached system would be computationally prohibitive. Therefore, it is necessary to provide a simplified model which can still yield an accurate, detailed solution for the solder. Since the solder balls have negligible effect on the deformation of the overall system, ABAQUS provides an ideal feature to fit this need: sub-modeling. This approach includes two subsequent analyses: a global analysis with a relatively coarse mesh used to simulate the whole 3D model of the PCB-solder-package assembly and a submodel analysis with a refined mesh to simulate the critical solder ball. These two analyses are linked together through transferring the time-dependent solutions saved in the global analysis to the relevant boundary nodes of the submodel. An outline of the procedures is shown schematically in Fig. 4. All of these modules, pre-process, solve, and post-process, are automated using ABAQUS python scripts. The four steps are described as follows:
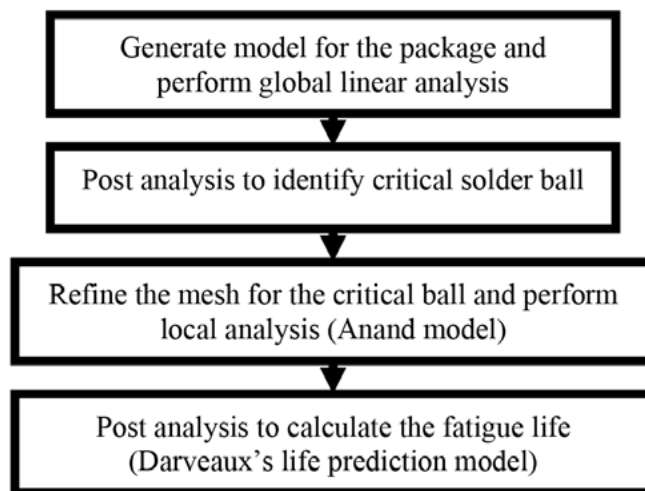

Fig. 4 Procedures for TC simulations

Source: Abaqus User Conference, 2007

1. The global modeling. The purpose of global modeling is to identify the critical local ball and to provide driving boundary conditions for the subsequent submodeling analysis. Because of the symmetry, only a quarter of the PCB-solder-package assembly is modeled. Only linear elastic properties are assumed for package materials. Quadratic elements are used, with a typical mesh shown in Fig. 5a.

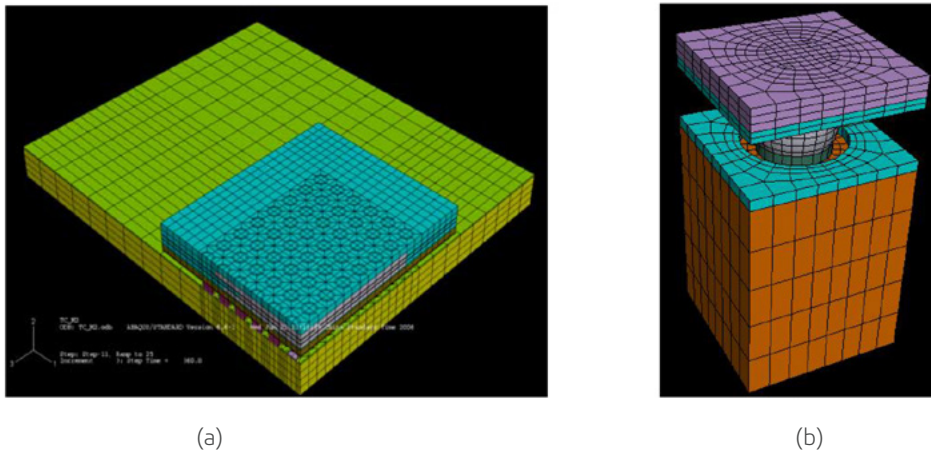(a)   (b)

Fig. 5 Finite element mesh for global (a) and local (b) models

2. Post global analysis. After the global analysis, an ABAQUS scripting interface is used to access the output database and to locate the solder ball with maximum Von-Misses stress. The position is then saved for next local modeling.

3. The submodeling. The local model includes only one critical solder joint with its location determined previously and part of the package and part of the board. The refined mesh is shown in Fig. 5b. The constitutive properties of the solder ball are captured by the Anand model. The driving boundary conditions are based on interpolation of the global solution around the vicinities of the critical solder ball.

4. Post local analysis. In this step, Darveaux' model is implemented to calculate the fatigue life of the solder ball. The accumulated creep energy density per cycle needs to be extract from the output database. To reduce stress concentration issues, volume-averaged energy density, DWave, is used which is given by:

$$\Delta W_{ave} = \frac{\sum dW_i V_i}{\sum V_i}$$

(8)

where dWi and Vi are the incremental creep energy density per cycle and the volume associated with element i, respectively. The volume used to calculate the averaged energy is chosen as two 25 micron thick layers of solder elements near package and board sides.

5. Numerical examples

Numerical examples are provided here to illustrate the methodology described above. Two new ballouts, 110 and 116 balls, are considered here, as compared with the old product (95 balls). The layouts for the solder ball are shown in Fig. 6, respectively. To evaluate the reliability, a 3 stacked-die package is chosen with the dimensions tabulated in Table 3.
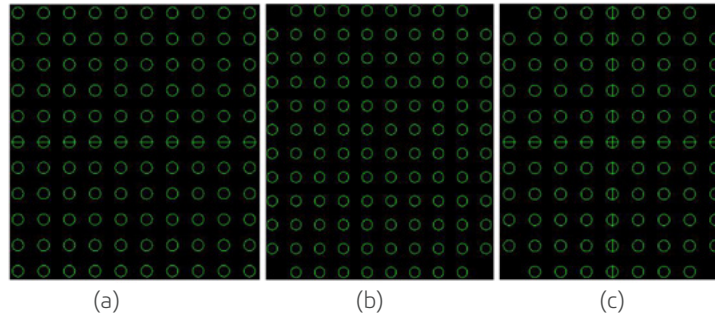
Source: Abaqus User Conference, 2007

Fig. 6 Ballout for (a) 110, (b) 116, and (c) 95 balls

(a)　　　　　　(b)　　　　　　(c)

Table 3 Dimensions (in mm) for the packages used in reliability evaluation

Package Size	Die Size	Mold Cap Thk	Sub Thk	Pitch	Ball Dia	Ball Height	Pad Type	Pad Size
9 x 10	6 x 8.2 x 0.125 5 x 8.5 x 0.125 7 x 8 x 0.125	0.65	0.2	0.8	0.4	0.25	SMD	0.45

The temperature profile used in the study is shown in Fig. 7. The thermal cycle is from −40°C to 125 °C, with a temperature ramp rate of 11°C/min ramp rate for 15 min. The dwell time at the low temperature and high temperature are both 15 min and the period is 1 h per cycle. Three cycles are simulated in both the global and local analyses.
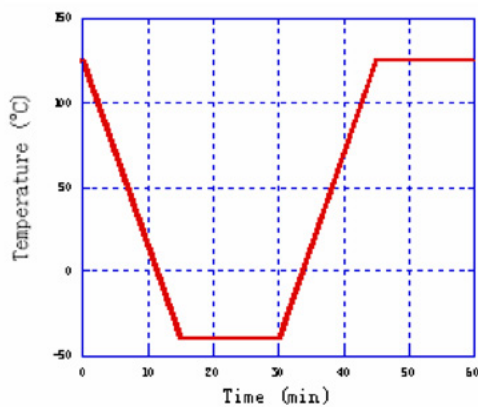

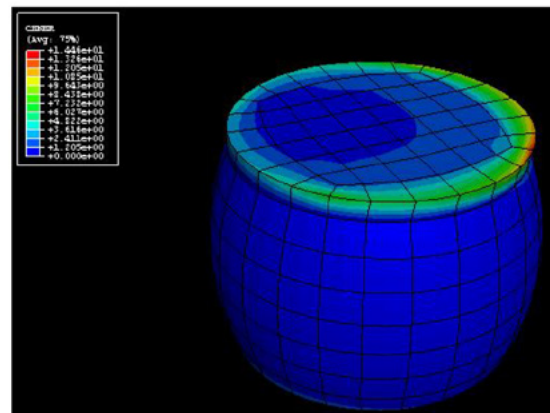Fig. 7 Temperature profile used in FEM calculations　　　Fig. 8 Contour plot of creep strain density

Fig. 8 shows the contour plot of creep strain density for the critical solder ball at the end of a cycle. As can be seen, the maximum density occurs near the package side, which is consistent with the experimental observations (see Fig. 3). The correctly predicted failure location also provides justification for the choice of control volumes for averaged density calculations. Figs. 9 show the accumulated creep strain density near the package and board sides per cycle for three cycles for ballout a, b and c, respectively. As can be seen, significant portion of the accumulated strain density is gained during ramp stages while the increment during dwell is negligible. For all of these three ballouts, creep strain density clearly shows asymptote after the 2nd cycle, but it has not yet quite saturated. Hence the accumulated strain densities near the package side after the 3rd cycle are used for fatigue life evaluation in Eqs. 5-7. The predicted failure cycles for ballout 110 and 105 are roughly the same (449 cycles for 110 balls and 452 cycles for 105 balls), but both of them are marginal worse than the 116 balls (476).
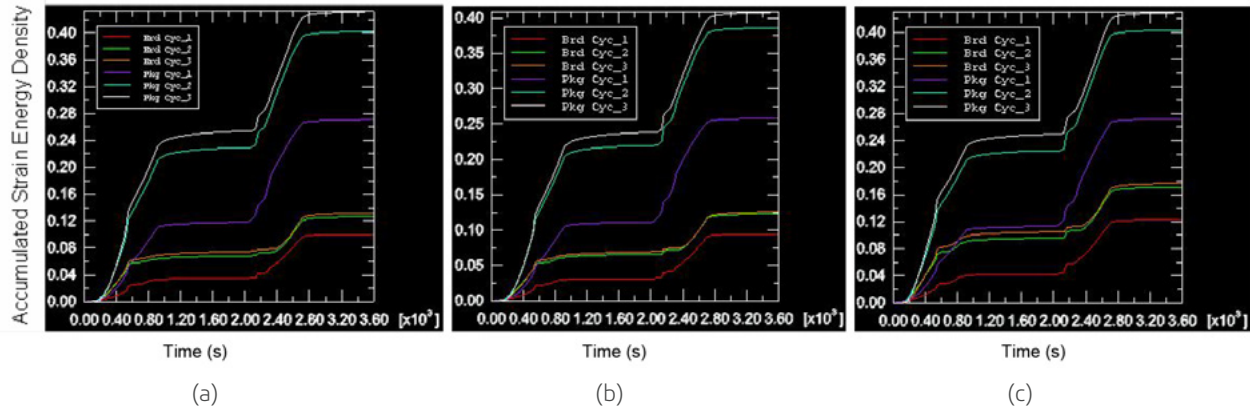
Fig. 9 Accumulated creep strain energy density per cycle for (a) 110, (b) 116, and (c) 95 balls

6. Conclusion

In this paper, Darveaux' model is implemented to study the thermal fatigue life of solder joints in BGA packages. Specifically, the Anand model, an ABAQUS built-in viscoplasticity model, is applied to represent the creep behavior for SAC405 solders. Global/local methodology is adopted to enhance computation efficiency. ABAQUS python scripting interfaces are used to generate the geometry mesh, perform analysis, and conduct post processing. The highly automated module provides a powerful tool for solder joint reliability analysis. Finally as a numerical example for capability demonstration, the implemented methodology is successfully applied to evaluate the temperature cycling reliability of three ballout designs.

7. Reference

1. ABAQUS manual version 6.6

2. Anand, L., "Constitutive Equations for Hot-Working of Metals," International Journal of Plasticity, Vol. 1, pp. 213-231, 1985.

3. Brown, S.B., K.H. Kim, and L. Anand, "An Internal Variable Constitutive Model for Hot Working of Metals," International Journal of Plasticity, Vol. 5, pp. 95-130, 1989.

4. Darveaux, R., "Effect of simulation methodology on solder joint crack growth correlation," in Proc. 50th Electronic Components and Technology Conf., May 2000, pp. 1048–1058.

5. Ghaffarian, Reza, "Accelerated Thermal Cycling and Failure Mechanisms for BGA and CSP Assemblies," Journal of Electronic Packaging, 2000, Volume 122, Issue 4, pp. 335-340.

6. Lau, J., and J. R. Rice, ''Thermal Stress/Strain Analyses of Ceramic Quad Flat Pack Packages and Interconnections,'' Proc. Elect. Components and Technology 40th Conf., Las Vegas, Nevada, 1990, Vol. 1, pp. 824–834.

7. Reinikainen, T.O., P. Marjadi, and J.K. Kivilahti, "Deformation Characteristics and Microstructural Evolution of SnAgCu Solder Joints," EuroSIME 6th International Conference, Germany, Apr. 2005, pp. 91-98.

8. Wiese, S., et al, "Microstructural Dependence of Constitutive Properties of Eutectic SnAg and SnAgCu Solders," 53rd ECTC ,2003, pp. 197-206.

Our 3DEXPERIENCE® **platform powers our brand applications, serving 12 industries, and provides a rich portfolio of industry solution experiences.**

Dassault Systèmes, the **3D**EXPERIENCE® Company, provides business and people with virtual universes to imagine sustainable innovations. Its world-leading solutions transform the way products are designed, produced, and supported. Dassault Systèmes' collaborative solutions foster social innovation, expanding possibilities for the virtual world to improve the real world. The group brings value to over 210,000 customers of all sizes in all industries in more than 140 countries. For more information, visit **www.3ds.com**.

3DEXPERIENCE®

DASSAULT SYSTEMES | The **3D**EXPERIENCE® Company